An Evaluation of Time Integration Schemes in the Solution of Contact Problems

by

Gunwoo Noh

Submitted to the Department of Mechanical Engineering
in partial fulfillment of the requirements for the degree of

Master of Science in Mechanical Engineering

at the

MASSACHUSETTS INSTITUTE OF TECHNOLOGY

February 2011

Author .....
Department of Mechanical Engineering
January 20, 2011

Certified by .....
Klaus-Jürgen Bathe
Professor
Thesis Supervisor

Accepted by ....
David E. Hardt
Chairman, Department Committee on Graduate Theses

An Evaluation of Time Integration Schemes in the Solution of Contact Problems

by

Gunwoo Noh

Submitted to the Department of Mechanical Engineering
on January 20, 2011, in partial fulfillment of the
requirements for the degree of
Master of Science in Mechanical Engineering

Abstract

Contact analysis is an important branch of structural mechanics. The finite element method has become a major solution approach because of the high nonlinearities in contact problems. A large number of algorithms have been proposed and extensively used to solve engineering problems, but some issues have not been addressed yet. The first purpose of this research is to evaluate attempts to achieve accurate and practical time integration schemes for contact problems. Towards this aim, this study proposes an analytical form of the solutions using the time integration schemes that can be used in the evaluation of different methods. Then, a simple velocity- and acceleration-update process that is combined with the conventional time integration methods is proposed to suppress (as much as possible) spuriously generated energy during the contact events.

Thesis Supervisor: Klaus-Jürgen Bathe
Title: Professor

Acknowledgments

I would like to express my deepest gratitude to my supervisor, Prof. Klaus-Jügen Bathe, for his guidance, support and patience. Without his enthusiasm, his inspiration, and his great efforts to explain things clearly, I would have been lost.

I am also thankful to all of my friends including all the members in the Finite Element Research Group who made my time at M.I.T. enjoyable.

This work was partially supported by Samsung Scholarship Foundation, which is gratefully acknowledged.

Lastly and most importantly, I wish to thank my family, my father, Sung-Hak Noh, my mother, Sun-Young Hwang, and my sister, Yoon-Ji Noh for their invaluable support.

Contents

List of Figures

Chapter 1

Introduction

1.1 Background

Contact and impact are common phenomena in many engineering fields when two or more objects try to occupy the same position. Wear and lubrication in the metal forming process, automobile crash tests and drilling in geological investigations are typical examples. Material nonlinearity, geometric nonlinearity and transient effects should be considered. In any analysis including contact events, it is evident that proper boundary conditions should also be considered.

However, one may notice that the exact contact interface is not known prior to the analysis in general. Since both tractions and displacements at the contact interface are a priori unknowns, the boundary conditions cannot be treated as simple Dirichlet or Neumann boundary conditions. Also, the motion of the objects in contact is not smooth at their contact interface. In other words, velocity fields of objects at the contact interface can jump [21][20]. Thus, contact problems fall into one of the most difficult categories of problems.

To consider transient effects in dynamic contact analysis, time integration is needed. Time integration algorithms can be divided into two categories: implicit approaches and explicit approaches. The explicit approach is relatively simple and easy to implement. Explicit approaches are largely used to solve various engineering problems [14][17]. However, explicit approaches are only conditionally stable and

often require a very small time step size to get reasonable results. In any analysis of contact events, it is also often required to make non-physical assumptions for the contact constraints. On the other hand, many implicit approaches are unconditionally stable in linear problems [16]. Therefore, a large time step size can be used for sufficient accuracy; this characteristic is a great advantage and has implications for many applications.

On the other hand, time integration methods that are unconditionally stable for linear dynamics often lose this stability in nonlinear cases [3]. The loss of stability can be treated as a loss of energy consistency in the system. Many researchers have made efforts to ensure the energy conservation of systems; their approaches can be classified into three categories [15]. The first group of algorithms introduces numerical damping to prevent response blow ups. These methods do not require additional computational cost and dissipate spurious high-frequency response selectively (discussed in chapter 2). However, these methods show excessive numerical dissipation when using too large a time step size. In the second category, methods enforce conservation of energy and momentum by using Lagrange multipliers. These methods typically exactly enforce energy-momentum conservation. However, since such methods require the solution of additional equations for every node, they can be computationally very expensive for large problems. In the third group, the algorithms enforce energy-momentum conservation algorithmically. They show very good performance from an energy-momentum conservation point of view. However, these methods solve equilibrium equations not at the discrete time points of interest. Also, for contact problems, since these methods enforce the velocity at contact surfaces rather than the constraint of impenetrability, the impenetrability condition is violated in general [18][19]. In short, the algorithm for nonlinear problems such as contact problems are still to be improved.

To obtain a better numerical method that is both accurate and efficient, it is important to specify the desired characteristics of the numerical method. One can find a great set of desired characteristics for numerical methods for general structural problems in the work of the ref. [2]. The set of the desired characteristics of the

methods in [2] is also valid for methods of contact problems. In addition, we need to consider the specific requirements for contact problems, such as contact constraints.

According to [1][2], it is desirable to have a method that solves the dynamic equilibrium equations at the discrete time points of interest. To solve equilibrium equations accuratly, it is natural to address them at the time point where the equilibrium equations are valid. For contact problems, this characteristic also has additional benefits. Specifically, we can exactly enforce a no-penetration condition using traditional approaches. When we solve an equation at the point of interest, it does not require additional computational cost for such items as weighted stress. We refer to [1] for the rest of the desired characteristics of accuracy, stability and efficiency for general structural problems.

However, for contact problems, energy consistency during contact events requires additional considerations. In approaches that solve dynamic equilibrium equations at discrete time points of interest, contact forces, which occur one step "before" the current time point, cause energy generation. This is because the energy change of the system depends on the average of the contact forces at the current time point and at the previous time point (discussed in chapter 4.2). This spuriously generated energy can cause the method to fail in problems that include contact events even if the time integration method is unconditionally stable in linear problems [18].

The Energy Momentum method, which uses the mid-point rule and solves dynamic equations at the midpoint of discrete time points of interest, succeeds in a unique way in making the energy change depend on only the contact force at the current time step [22]. Since there is no effect of the contact force at the previous time step, this method naturally succeeds at eliminating the spuriously generated energy and achieves the energy consistency of the system. Although it has some disadvantages, it is possible that this aspect will be a critical one that will make methods in the category of Energy Momentum powerful.

1.2 Motivations

For practical usage for contact problems, we would like to have a method that

1) solves the equilibrium equation 'at' the discrete time points of interest,

2) meets the energy conservation in general problems, which include contact events

3) meets the no penetration condition exactly,

4) does not introduce additional variables, like additional Lagrange multipliers, to conventional methods.

When a method solves an equilibrium equation at the discrete time points of interest with consideration of the contact constraints, it is possible to meet the no penetration condition exactly using conventional approaches.

However, to meet the energy consistency condition, a method should be able to handle the energy generation from the contact forces, which is an inevitable phenomena when we solve the equilibrium equations at the discrete time points of interest. At the same time, from a viewpoint of practical engineering, we do not want to introduce any additional variables or additional iterations to handle this spuriously generated energy. In this study, we will investigate and evaluate existing time integration methods in order to improve them to be used in contact problems satisfying the conditions above.

1.3 Outline of the thesis

This thesis is organized as follows. In chapter 2, a widely used time integration method for general engineering problems, the Bathe method, is reviewed. The stability and the accuracy characteristics of the method are discussed. chapter 3 introduces an analytical form to measure the accuracy of time integration methods in terms of amplitude decay and period elongation. By using the proposed analytical form, the accuracy characteristics of time integration schemes with respect to the initial conditions of the contact events is investigated. In chapter 4, we study the effect of contact forces on the total energy change in the solutions using implicit time integra-

tion methods. Based on the contact force analysis, a simple velocity and acceleration update process is proposed and numerical examples are presented.

Chapter 2

Bathe method

The method is a combination of the trapezoidal rule and the three point backward Euler method. Although the basic difference formulas were of course applied earlier, see for example [8] and for example Bank et. al. for first-order systems in electrical engineering [9], we call the method the Bathe method, because KJ Bathe applied the method first to second-order structural dynamics and discovered the powerful properties in such time integration solutions [3][2]. In the following sections, we study the stability and the accuracy characteristics of the method.

2.1 Direct integration approximation and load operators

Using the same time step size Δt, the results of direct integration methods are equivalent to the results of the mode superposition method which changes the basis of equilibrium equations to modal displacements and solves n decoupled equilibrium equations. Therefore, to analyze the methods, we only need to analyze one equilibrium equation presented in the modal displacement basis. Then, based on the direct integration approximation and the load operators of the equilibrium equation presented in the modal displacement basis, we can see the stability characteristics of the method by obtaining the spectral radii [1].

In the first sub-step, the trapezoidal rule is used and we consider the equilibrium state at time $t + \Delta t/2$

$$ {}^{t+\Delta t/2}\ddot{x} + 2\xi\omega^{t+\Delta t/2}\dot{x} + \omega^{2t+\Delta t/2}x = {}^{t+\Delta t/2}r \tag{2.1} $$

$$ {}^{t+\Delta t/2}\dot{x} = {}^{t}\dot{x} + \frac{{}^{t}\ddot{x} + {}^{t+\Delta t/2}\ddot{x}}{4}\Delta t \tag{2.2} $$

$$ {}^{t+\Delta t/2}x = {}^{t}x + \frac{{}^{t}\dot{x} + {}^{t+\Delta t/2}\dot{x}}{4}\Delta t \tag{2.3} $$

Substituting ${}^{t+\Delta t/2}\dot{x}$ and ${}^{t+\Delta t/2}x$ into (2.1), we can solve for ${}^{t+\Delta t/2}\ddot{x}$ and then use (2.2) and (2.3) to calculate ${}^{t+\Delta t/2}\dot{x}$ and ${}^{t+\Delta t/2}x$. Then, we can establish

$$ \begin{bmatrix} {}^{t+\Delta t/2}\ddot{x} \\ {}^{t+\Delta t/2}\dot{x} \\ {}^{t+\Delta t/2}x \end{bmatrix} = \mathbf{A_1} \begin{bmatrix} {}^{t}\ddot{x} \\ {}^{t}\dot{x} \\ {}^{t}x \end{bmatrix} + \mathbf{L_1}\,{}^{t+\Delta t/2}r \tag{2.4} $$

where

$$ \mathbf{A_1} = \frac{1}{\alpha} \begin{bmatrix} -8\,\xi\,\omega\,\Delta t - \omega^2\Delta t^2 & -32\,\xi\,\omega - 8\,\omega^2\Delta t & -16\,\omega^2 \\ 4\,\Delta t & 16 - \omega^2\Delta t^2 & -4\,\omega^2\Delta t \\ \Delta t^2 & 8\,\Delta t + 2\,\Delta t^2\xi\,\omega & 16 + 8\,\xi\,\omega\,\Delta t \end{bmatrix} \tag{2.5} $$

$$ \mathbf{L_1} = \frac{1}{\alpha} \begin{bmatrix} 16 \\ 4\,\Delta t \\ \Delta t^2 \end{bmatrix} \tag{2.6} $$

$$ \alpha = 16 + 8\,\xi\,\omega\,\Delta t + \omega^2\Delta t^2 \tag{2.7} $$

In the following second sub-step, the three-point Euler backward formula is used and the equilibrium state at time $t + \Delta t$ is expressed as

$$ {}^{t+\Delta t}\ddot{x} + 2\xi\omega^{t+\Delta t}\dot{x} + \omega^{2t+\Delta t}x = {}^{t+\Delta t}r \tag{2.8} $$

$$ {}^{t+\Delta t}\dot{x} = \frac{{}^{t}x}{\Delta t} - \frac{4^{t+\Delta t/2}x}{\Delta t} + \frac{3^{t+\Delta t}x}{\Delta t} \tag{2.9} $$

$$ {}^{t+\Delta t}\ddot{x} = \frac{{}^{t}\dot{x}}{\Delta t} - \frac{4^{t+\Delta t/2}\dot{x}}{\Delta t} + \frac{3^{t+\Delta t}\dot{x}}{\Delta t} \tag{2.10} $$

Substituting ${}^{t+\Delta t}\dot{x}$ and ${}^{t+\Delta t}\ddot{x}$ into (2.7) and using the solution from the first step, we can solve for ${}^{t+\Delta t}x$ and then use (2.8) and (2.9) to calculate ${}^{t+\Delta t}\dot{x}$ and ${}^{t+\Delta t}\ddot{x}$. It leads to

$$ \begin{bmatrix} {}^{t+\Delta t}\ddot{x} \\ {}^{t+\Delta t}\dot{x} \\ {}^{t+\Delta t}x \end{bmatrix} = \mathbf{A_2} \begin{bmatrix} {}^{t+\Delta t/2}\ddot{x} \\ {}^{t+\Delta t/2}\dot{x} \\ {}^{t+\Delta t/2}x \end{bmatrix} + \mathbf{A_3} \begin{bmatrix} {}^{t}\ddot{x} \\ {}^{t}\dot{x} \\ {}^{t}x \end{bmatrix} + \mathbf{L_2}\,{}^{t+\Delta t}r \tag{2.11} $$

where

$$ \mathbf{A_2} = \frac{1}{\beta} \begin{bmatrix} 0 & -24\,\xi\,\omega - 4\,\omega^2\,\Delta t & -12\,\omega^2 \\ 0 & 12 & -4\,\omega^2\,\Delta t \\ 0 & 4\,\Delta t & 12 + 8\,\xi\,\omega\,\Delta t \end{bmatrix} \tag{2.12} $$

$$ \mathbf{A_3} = \frac{1}{\beta} \begin{bmatrix} 0 & 6\,\xi\,\omega + \omega^2\,\Delta t & 3\,\omega^2 \\ 0 & -3 & \omega^2\,\Delta t \\ 0 & -\Delta t & -3 - 2\,\xi\,\omega\,\Delta t \end{bmatrix} \tag{2.13} $$

$$ \mathbf{L_2} = \frac{1}{\beta} \begin{bmatrix} 9 \\ 3\,\Delta t \\ \Delta t^2 \end{bmatrix} \tag{2.14} $$

$$ \beta = 9 + 6\,\xi\,\omega\,\Delta t + \omega^2\,\Delta t^2 \tag{2.15} $$

After substituting (2.4) into (2.11), the direct integration approximation and the load operator for one time step are obtained

$$\begin{bmatrix} {}^{t+\Delta t}\ddot{x} \\ {}^{t+\Delta t}\dot{x} \\ {}^{t+\Delta t}x \end{bmatrix} = \mathbf{A_2} \left(\mathbf{A_1} \begin{bmatrix} {}^{t}\ddot{x} \\ {}^{t}\dot{x} \\ {}^{t}x \end{bmatrix} + \mathbf{L_1}\,{}^{t+\Delta t/2}r \right) + \mathbf{A_3} \begin{bmatrix} {}^{t}\ddot{x} \\ {}^{t}\dot{x} \\ {}^{t}x \end{bmatrix} + \mathbf{L_2} + {}^{t+\Delta t}r \tag{2.16}$$

$$\begin{bmatrix} {}^{t+\Delta t}\ddot{x} \\ {}^{t+\Delta t}\dot{x} \\ {}^{t+\Delta t}x \end{bmatrix} = (\mathbf{A_2 A_1} + \mathbf{A_3}) \begin{bmatrix} {}^{t}\ddot{x} \\ {}^{t}\dot{x} \\ {}^{t}x \end{bmatrix} + \mathbf{A_2 L_1}\,{}^{t+\Delta t/2}r + \mathbf{L_2} + {}^{t+\Delta t}r \tag{2.17}$$

Therefore,

$$\begin{bmatrix} {}^{t+\Delta t}\ddot{x} \\ {}^{t+\Delta t}\dot{x} \\ {}^{t+\Delta t}x \end{bmatrix} = \mathbf{A} \begin{bmatrix} {}^{t}\ddot{x} \\ {}^{t}\dot{x} \\ {}^{t}x \end{bmatrix} + \mathbf{L_a}\,{}^{t+\Delta t/2}r + \mathbf{L_b}\,{}^{t+\Delta t}r \tag{2.18}$$

where

$$\mathbf{A} = \mathbf{A_2 A_1} + \mathbf{A_3}$$

$$= \frac{1}{\alpha\beta} \begin{bmatrix} -4\,\omega\,dt\,(24\,\xi + 7\,\omega\,dt) & \omega\,\left(-288\,\xi + 14\,\xi\,\omega^2 dt^2 - 144\,\omega\,dt + 5\,\omega^3 dt^3 + 48\,\xi^2 \omega\,dt\right) \\ -4\,dt\,\left(-12 + \omega^2 dt^2\right) & 144 - 47\,\omega^2 dt^2 - 8\,\xi\,\omega^3 dt^3 - 24\,\xi\,\omega\,dt \\ 4\,dt^2\,(7 + 2\,\xi\,\omega\,dt) & dt\,\left(144 - 5\,\omega^2 dt^2 + 80\,\xi\,\omega\,dt + 16\,\xi^2 \omega^2 dt^2\right) \end{bmatrix}$$

$$\begin{bmatrix} \omega^2\left(24\,\xi\,\omega\,dt + 19\,\omega^2 dt^2 - 144\right) \\ \omega^2 dt\,\left(-96 - 24\,\xi\,\omega\,dt + \omega^2 dt^2\right) \\ -19\,\omega^2 dt^2 + 144 + 168\,\xi\,\omega\,dt + 48\,\xi^2 \omega^2 dt^2 - 2\,\xi\,\omega^3 dt^3 \end{bmatrix} \tag{2.19}$$

$$\mathbf{L_a} = \mathbf{A_2 L_1} = \frac{1}{\alpha\beta} \begin{bmatrix} -4\omega\, dt\ (24\xi + 7\omega\, dt) \\ -4\, dt\ \left(-12 + \omega^2 dt^2\right) \\ 4\, dt^2\, (7 + 2\xi\omega\, dt) \end{bmatrix} \tag{2.20}$$

$$\mathbf{L_b} = \mathbf{L_2} = \frac{1}{\beta} \begin{bmatrix} 9 \\ 3\, dt \\ dt^2 \end{bmatrix} \tag{2.21}$$

In the direct integration for nonlinear analysis, the Bathe method is about twice as expensive as the trapezoidal rule.

2.1.1 Stability and Accuracy

The Bathe method is in linear analysis unconditionally stable and second-order accurate because so are the trapezoidal rule and the three-point backward difference method [3][24]. Also, in references [2][23], the method remains stable when the trapezoidal rule is not effective. This is because the Bathe method uses the three-point backward Euler method in the second sub step which introduces a small amount of numerical damping.

The spectral radii is obtained from the direct integration operator in equation (2.18). Fig.2-1 shows that the Bathe method has numerical damping, in particular when $\Delta t/T$ is larger than 1 where numerical integration methods cannot get any accuracy.

By using the approach in reference [5], the period elongation and the amplitude decay are obtained. For evaluation, responses of simple spring mass systems without physical damping or external forces as function of $\Delta t/T$ are investigated where Δt is the time step size and T is the natural frequency of the system. The initial condition for the mass is a unit displacement and zero velocity. Figures 2-3 and 2-4 show that the period elongation and the amplitude decay of the trapezoidal rule and the Bathe method.

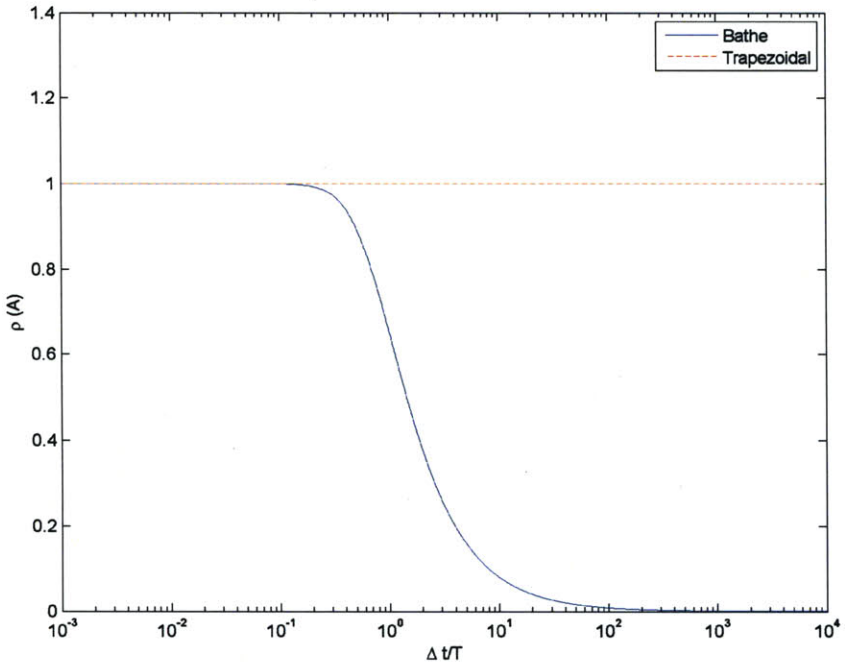

Figure 2-1: Spectral radii of approximation oprators, no physical damping case

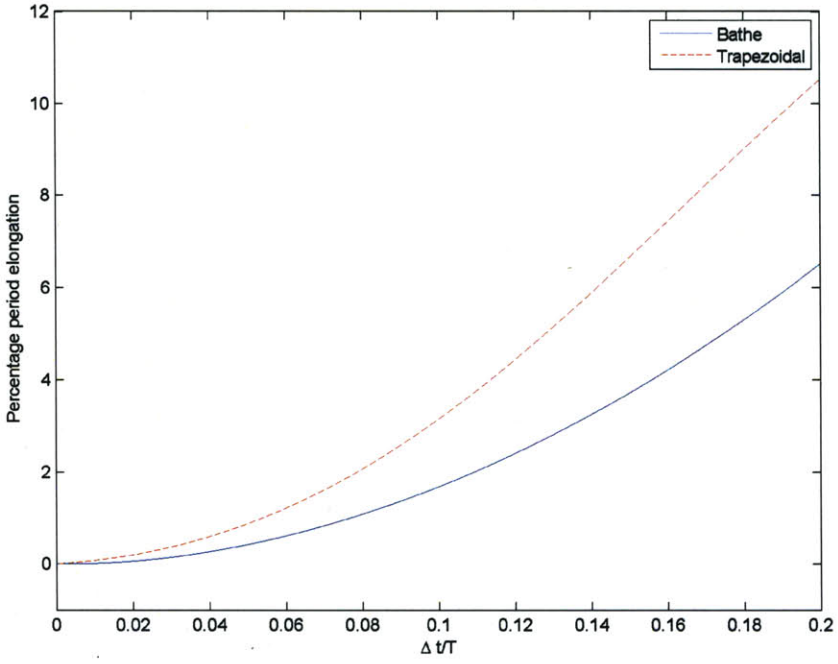

Figure 2-2: Percentage period elongation

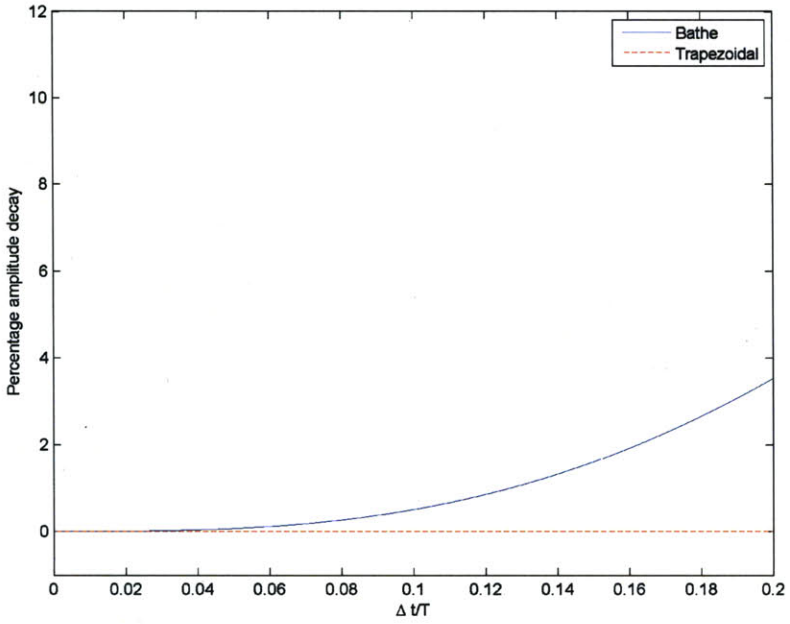

Figure 2-3: Percentage amplitude decay

Chapter 3

Accuracy characteristics of time integration schemes in contact problems

Many direct integration methods have been developed and investigated. Amplitude decay and period elongation have been widely used as parameters to describe the stability and accuracy characteristics of these direct integration methods. However, there is no strict procedure that can be used to decide which method to use. A simple and efficient procedure is presented here that can help to understand the characteristics of a method for contact problems.

The accuracy of a method in relation to contact problems can be measured in many different ways. The L^1 norm, which is the most widely used parameter for accuracy, simply represents the differences between the values of the results at each time step. Therefore, it cannot include important information that can represent accuracy in many contact problems, such as the distortion of the shape of response and the degree of the shift of the response. Therefore, we use the difference of the first contact time as a parameter that measures accuracy, which significantly affects the total response of the system.

The response of a single degree of freedom problem from direct integration methods can be represented as a single trigonometric function by using its amplitude decay

and period elongation. Therefore, the contributions of the amplitude decay and period elongation on accuracy have been investigated by using this single function. The analytical form presented here can also be effective in current research efforts of developing better integration methods. For example, to develop a certain integration method, which has the desired accuracy and stability characteristics from the combination of two different methods, the accuracy characteristics of each method from this procedure can be helpful.

3.1 Analytical form of accuracy of a time integration method

To get a sense of the integration accuracy, the response of a single degree of freedom problem with no damping and no loading is often evaluated. The analytical solution of this typical problem with initial conditions $x_0 = A_0$, $\dot{x} = 0$, $\ddot{x} = \omega^2 A_0$ is

$$A_0 sin(\frac{2\pi}{T_0} + \phi) \tag{3.1}$$

where $T_0 = \frac{2\pi}{\omega}$, $\phi = -\frac{\pi}{2}$. However, when this problem is solved by a numerical integration method with period elongation and amplitude decay, the response is of the following form

$$A^* sin(\frac{2\pi}{T^*} + \phi) \tag{3.2}$$

where we can notice the A^* and T^* are

$$T^* = T_0 * (1 + \frac{PE}{100}) \tag{3.3}$$

$$A^* = A_0 * (1 - \frac{AD}{100})^{\frac{t}{T^*}} \tag{3.4}$$

Note that the effective period, T^*, is a constant throughout the entire simulation, while the effective amplitude, A^*, is exponentially related to time. Figure 3-1 shows that the periods of every oscillation of the calculated responses from the Bathe method

and the trapezoidal rule have the same value as T^*. The numerical solutions are calculated for $\Delta t/T_0 = 0.2$. The effective amplitude, A^* , is also calculated using each method's period elongation and amplitude decay at $\Delta t/T_0 = 0.2$. Figure. 3-2 shows the amplitudes at every oscillation. Since the trapezoidal rule has no amplitude decay, the amplitudes remain constant. However, the amplitudes of response from the Bathe method show that they are exponentially related to the simulation time. Again, the numerical solutions are calculated when the $\Delta t/T_0 = 0.2$ and A^* is calculated by using each method's period elongation and amplitude decay at $\Delta t/T_0 = 0.2$. Figure 3-3 and Figure 3-4 show that the analytical form of the solution with its period elongation and amplitude decay accurately represent the solutions from the integration methods, even after a long time. Of course, these properties (i.e. Eqs.(3.3) and (3.4)) simply hold because we consider a linear problem.

However, it should be recognized that the value of the integration methods' amplitude decay and period elongation, which are used in their analytical forms, are slightly different from the values used by the method in [5]. To make the analytical forms represent the calculated results precisely, we adjusted the values from the method in [5] and used the adjusted values. These adjusted values are the exact amplitude decay and period elongation. The difference in values from using the method in [5] comes from the interpolation step that finds the maximum point between the calculated points as stated in [5]. It can be easily understood that the error grows as the $\Delta t/T_0$. grows since the error from interpolation grows.

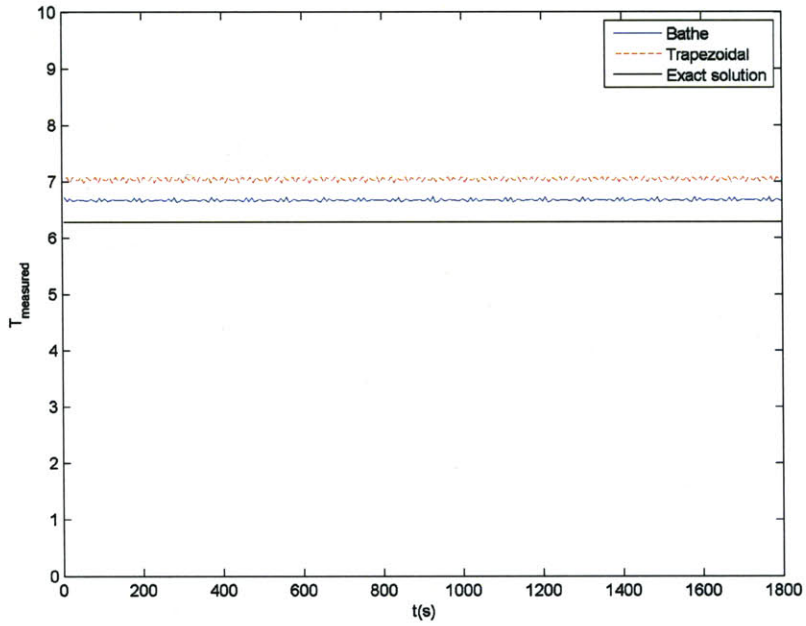

Figure 3-1: Periods of each oscillation of the solutions of the direct integration methods

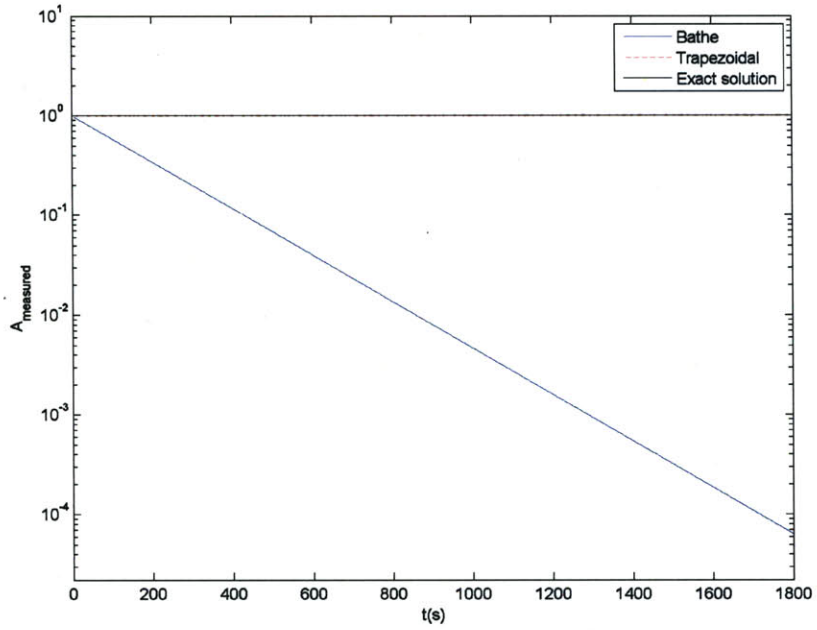

Figure 3-2: Amplitude of each oscillation of the solutions of the direct integration methods

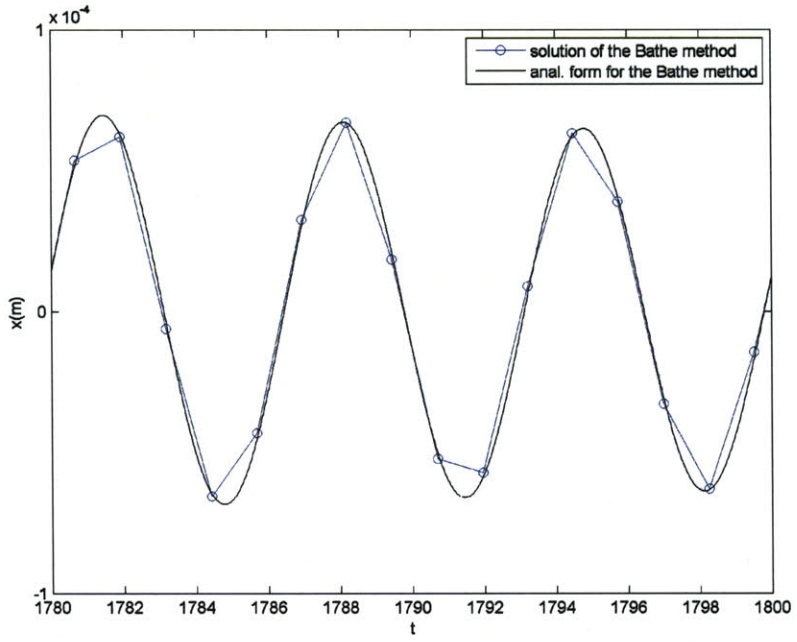

Figure 3-3: A solution of the Bathe method and a solution from its analytical form at $\Delta t/T = 0.2$.

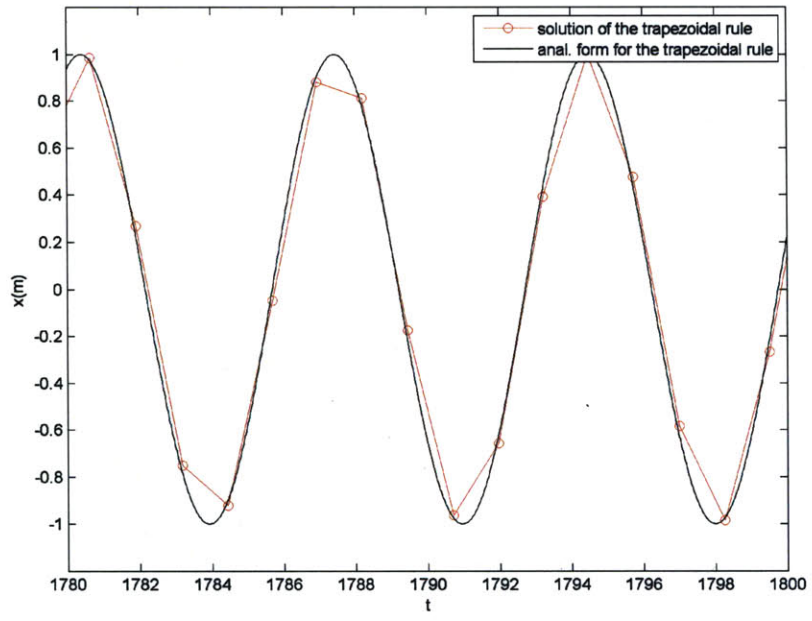

Figure 3-4: A solution of the trapezoidal rule and a solution from its analytical form at $\Delta t/T = 0.2$.

3.2 An accuracy analysis for contact problems

The accuracy of a method in contact problems can be measured in many different ways. The L^1 norm is the most widely used parameter that measures accuracy. However, it simply represents the differences between the values of the results at each time step. Therefore, in many cases, it cannot include important information that can represent accuracy in certain problems.

Therefore, besides using the L^1 norm as an estimator of errors, there have been many studies that have tried to find a good error estimator that shows the accuracy of the response. For the contact problems, the energy-momentum conservation and inter-penetration condition have been widely used as parameters that measure the accuracy of the contact algorithm [25]. These conditions are good in seeing whether the response follows the laws of physics. However, these conditions, such as energy-momentum conservation, only see the properties of the total system instead of the individual contact objects. Therefore, when we are interested in not only the overall accuracy of the response of the total system, but also in detailed predicitons and the behavior of the individual objects, these conditions are not effective.

In this sense, the conditions at each contact can be a good error estimator for certain contact problems since these conditions determine the response after contact and determine the amount of the momentum exchange between the contacting bodies. Therefore, we notice that the accuracy of the contact conditions affect the accuracy of the entire response.

In this section, by using the analytical form of the response from the previous section, we investigate the accuracy characteristics of the time integration methods in contact problems with a focus on the accuracy of the conditions seen at contact.

3.2.1 Error from the initial condition of the contact

To get an idea of the effect of the amplitude decay and period elongation of the time integration method, we consider a simple contact problem (Fig. 3-5). In this problem, we want to obtain the difference of the velocities of the ball when it contacts with the rigid wall. The ball has the equilibrium point at the origin. Initially, the ball is placed at the origin, moving at a velocity of $\frac{2\pi}{T_0}x_0$. The exact solution of the response of the rigid ball before contact is

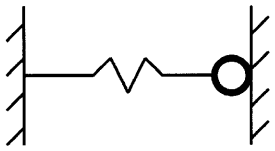

Figure 3-5: 1-D spring problem

$$x_e = x_0 \sin(\frac{2\pi}{T_0}t) \tag{3.5}$$

$$\dot{x_e} = \frac{2\pi}{T_0}x_0 \cos(\frac{2\pi}{T_0}t) \tag{3.6}$$

In this problem, the rigid wall appears sometime between $\frac{T}{2}(2n)$ and $\frac{T}{2}(2n+1)$ when $n = 0, 1, 2, \cdots$ so that the contacts happen at the times t_c where

$$t_c = \frac{T}{2}(2n+1) \qquad n = 0, 1, 2, \cdots \tag{3.7}$$

Therefore, the velocity of the ball just before the contact is

$$\dot{x_e}\,|_{t_c} = -\frac{2\pi}{T_0}x_0 \tag{3.8}$$

When the problem is solved by time integration methods which have amplitude decay and period elongation, the response of the ball before contact is

$$x^* = x_0^* \sin(\frac{2\pi}{T^*}t) \tag{3.9}$$

where

$$x_0^* = x_0(1 - \frac{AD}{100})^{\frac{t}{T^*}} = x_0 a \tag{3.10}$$

$$T^* = T_0(1 + \frac{PE}{100}) = T_0 b \tag{3.11}$$

Therefore, the contact time becomes

$$t_c^* = \frac{T^*}{2}(2n + 1) = t_c b \tag{3.12}$$

Also, from the equation (3.9), the velocity of the ball before contact becomes

$$\dot{x}^* = -\frac{x_0}{T_0 b} a^{\frac{t}{T^*}} (\ln(a) \sin(\frac{2\pi t}{T_0 b}) + 2\pi \cos(\frac{2\pi t}{T_0 b})) \tag{3.13}$$

Therefore, the velocity of the ball just before the contact (initial condition of the contact) is

$$\dot{x}^* \mid_{t_c^*} = \dot{x_e} \mid_{t_c} \frac{a^{\frac{1}{2}(2n+1)}}{b}$$

$$\dot{x}^* \mid_{t_c^*} = \dot{x_e} \mid_{t_c} (1 - \frac{AD}{100})^{\frac{1}{2}(2n+1)} (1 + \frac{PE}{100})^{-1} \tag{3.14}$$

Figure 3-8, 3-9 show the ratios of initial velocities of the ball at contact, $\frac{\dot{x}^* \mid_{t_c^*}}{\dot{x_e} \mid_{t_c}}$.

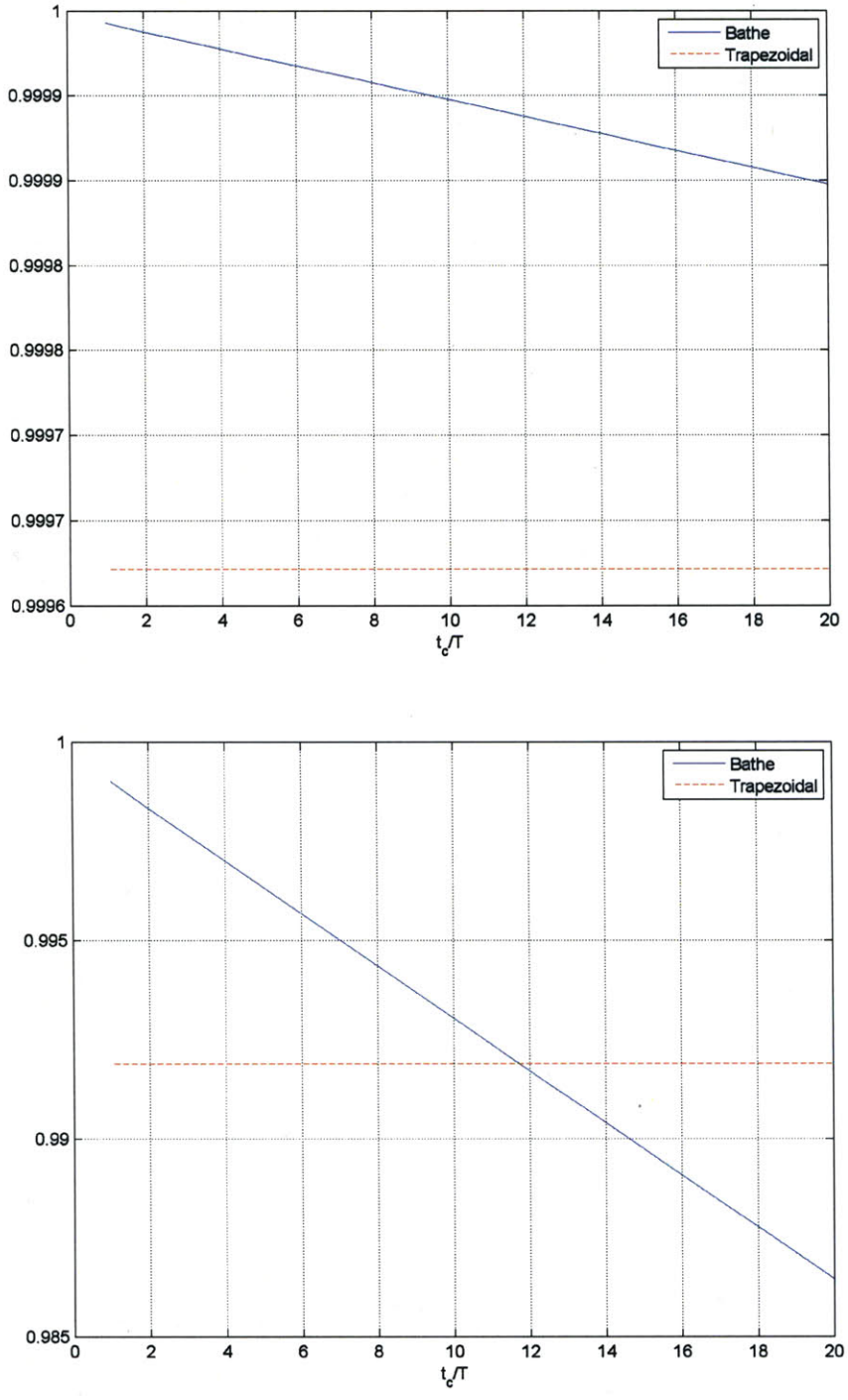

Figure 3-6: Ratios of initial velocity in contact from direct integration methods, $\frac{\dot{x}^*|_{t_c^*}}{\dot{x}_e|_{t_c}}$. case $\Delta t/T = 0.01,\ 0.05$.

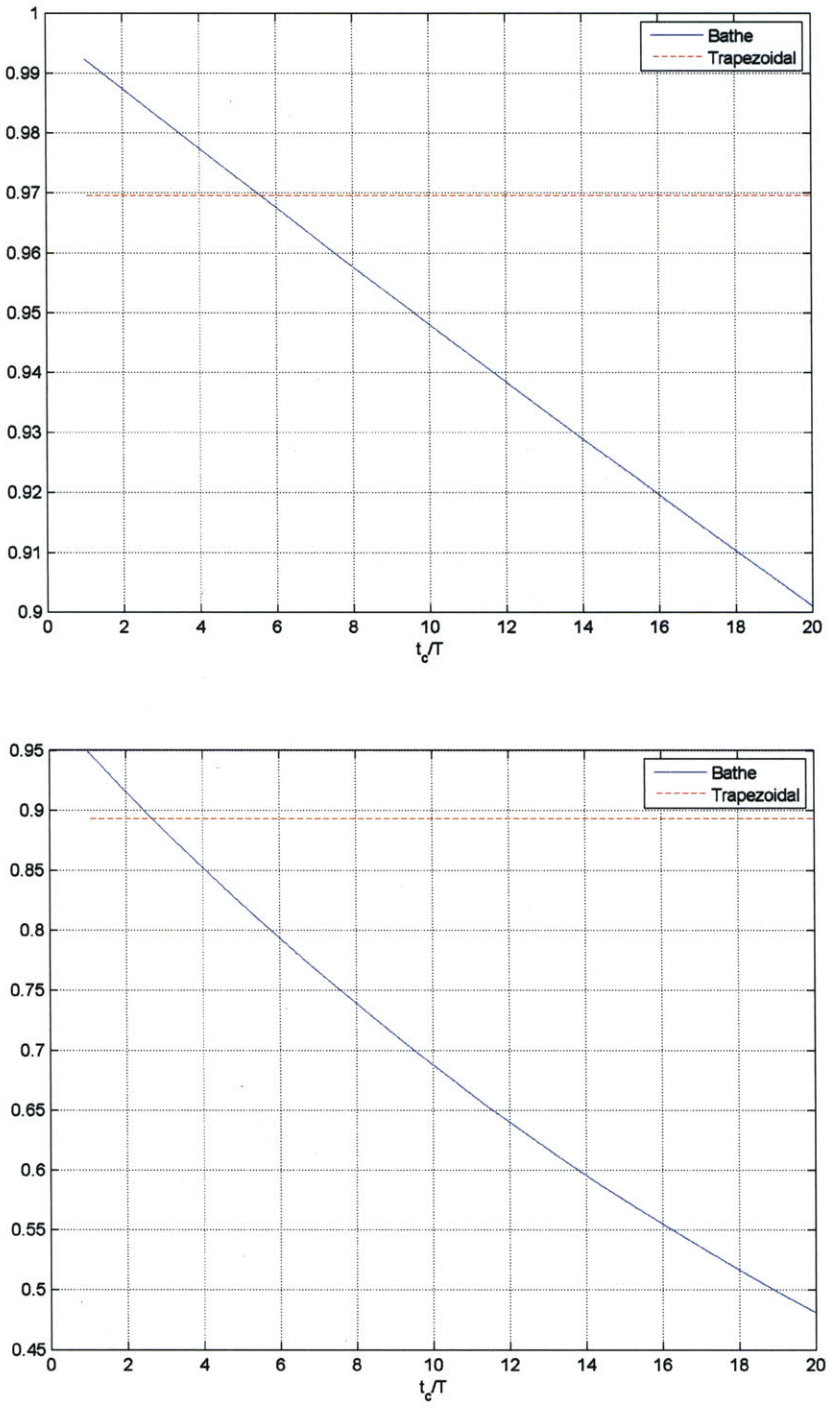

Figure 3-7: Ratios of initial velocity in contact from direct integration methods, $\frac{\dot{x}^*|_{t_c^*}}{\dot{x}_e|_{t_c}}$. case $\Delta t/T = 0.1,\ 0.2$.

Chapter 4

A simple contact algorithm for energy-momentum conservation

In contact problems, the contact force on each body appears and disappears abruptly and its amount and location are unknown a priori. Therefore, even for simple problems where the only nonlinearity comes from the events of contact, it is hard to assess the stability of an algorithm by using ideas of spectral radii, amplitude decay, or period elongation, as we did in the previous chapters.

However, when we study the energy variation of the system in each time step, we can see the influence of the events of contact and the generic characteristics of time integration methods. Also, we find that in the time step, when new contact occurs, the contact force causes the energy to decrease, while in the releasing step, when the contact disappears, the contact force causes the energy to increase. These facts motivate ways to eliminate the effect of the contact events on the system's energy by dealing with the contact force.

In this chapter, we investigate the energy change of the system by using the solution of two widely used implicit time integration methods: the Newmark method and the Bathe method. We also propose a simple way to remove the energy change due to the contact events by considering the work done by the contact force at that time step and by applying the concept of momentum exchange.

4.1 Energy change in implicit time integration methods in contact problems

To see the influence of the contact events on the total system energy, we can consider a simple linear system whose governing equation is

$$\mathbf{M}^{t+\Delta t}\ddot{U} + \mathbf{K}^{t+\Delta t}U = {}^{t+\Delta t}\mathbf{R_c} \tag{4.1}$$

To focus on the effect of the contact events, we can assume that the nonlinearity comes only from the contact events. In this simple model system, the M and K matrices are all constant, symmetric and semi definite. To solve this system implicitly , we apply two widely used time integration methods : the Newmark method and the Bathe method. We investigate the energy change in each time step by a similar approach as proposed in [12]. To simplify the algebra, we use the following four operators.

$$< {}^{t}(X) >= 1/2({}^{t+\Delta t}(X) + {}^{t}(X)) \tag{4.2}$$

$$[{}^{t}(X)] = ({}^{t+\Delta t}(X) - {}^{t}(X)) \tag{4.3}$$

$$\mathbf{T}(X) = 1/2(X)^T\mathbf{M}(X) \tag{4.4}$$

$$\mathbf{V}(X) = 1/2(X)^T\mathbf{K}(X) \tag{4.5}$$

4.1.1 Newmark Method

The following assumptions are used in the Newmark method

$${}^{t+\Delta t}\dot{U} = {}^{t}\dot{U} + ((1-\delta){}^{t}\ddot{U} + \delta {}^{t+\Delta t}\ddot{U})\Delta t \tag{4.6}$$

$${}^{t+\Delta t}U = {}^{t}U + {}^{t}\dot{U}\Delta t + ((\frac{1}{2} - \alpha){}^{t}\ddot{U} + \alpha\ddot{U})\Delta t^2 \tag{4.7}$$

Using the conventions we defined before, we can express the above equations as

$$[{}^t\dot{U}] =< {}^t\ddot{U} > +\Delta t(\delta - \frac{1}{2})[{}^t\ddot{U}] \tag{4.8}$$

$$[{}^tU] = \Delta t <^t \dot{U} > +\Delta t^2(\alpha - \frac{\delta}{2})[{}^t\ddot{U}] \tag{4.9}$$

The energy change of the total system in each time step, $[{}^tE]$, is the sum of the change of the kinetic energy, $[\mathbf{T}({}^t\dot{U})]$, and the change of the strain energy, $[\mathbf{V}({}^tU)]$ where

$$\begin{aligned}
[\mathbf{T}({}^t\dot{U})] &= [{}^t\dot{U}]^T\mathbf{M} <^t \dot{U} > \\
&= (<^t \ddot{U} >^T +(\delta - \frac{1}{2})[{}^t\ddot{U}]^T)\mathbf{M}([{}^tU] - \Delta t^2(\alpha - \frac{\delta}{2})[{}^t\ddot{U}]) \qquad (4.10)\\
[\mathbf{V}({}^tU)] &= [{}^tU]^T\mathbf{K} <^t U > \qquad (4.11)
\end{aligned}$$

Therefore, the change of the total system energy is

$$\begin{aligned}
[{}^tE] &= [\mathbf{T}({}^t\dot{U})] + [\mathbf{V}({}^tU)] \\
&= <^t \ddot{U} >^T \mathbf{M}[{}^tU] + (\delta - \frac{1}{2})[{}^t\ddot{U}]^T\mathbf{M}[{}^tU] \\
&\quad -\Delta t^2(\alpha - \frac{\delta}{2}) <^t \ddot{U} >^T \mathbf{M}[{}^t\ddot{U}] - \Delta t^2(\alpha - \frac{\delta}{2})(\delta - \frac{1}{2})[{}^t\ddot{U}]^T\mathbf{M}[{}^t\ddot{U}] \\
&\quad +[{}^tU]^T\mathbf{K} <^t U > \qquad (4.12)
\end{aligned}$$

Also, we can find the following relations from equation (4.1)

$$<^t \ddot{U} >^T \mathbf{M}[{}^tU]+ <^t U >^T \mathbf{K}[{}^tU] =<^t \mathbf{R_c} >^T [{}^tU] \tag{4.13}$$

$$[{}^t\ddot{U}]^T\mathbf{M}[{}^tU] + [{}^tU]^T\mathbf{K}[{}^tU] = [{}^t\mathbf{R_c}]^T[{}^tU] \tag{4.14}$$

Using the above relations, we can simplify equation (4.12)

$$\begin{aligned}
[^tE] &= (<^t \mathbf{R_c}> + (\delta - \frac{1}{2})[^t\mathbf{R_c}])^T[^tU] \\
&\quad -\Delta t^2(\alpha - \frac{\delta}{2})[\mathbf{T}(^t\ddot{U})] - 2(\delta - \frac{1}{2})\mathbf{V}([^t\ddot{U}]) \\
&\quad -\Delta t^2(2\alpha - \delta)(\delta - \frac{1}{2})\mathbf{T}([^t\ddot{U}])
\end{aligned} \tag{4.15}$$

We can choose the variables α and δ. If we choose $\alpha = \frac{1}{4}$ and $\delta = \frac{1}{2}$ (the trapezoidal rule) equation (4.15) becomes

$$[^tE] = <^t \mathbf{R_c}>^T [^tU] \tag{4.16}$$

As we can see in the above equation, the average of the contact force at the current time and at the previous time causes the energy change. Also, as we expected, the total energy of the system is conserved if there is no contact. On the other hand, when we choose $\alpha = \frac{1}{2}$ and $\delta = \frac{1}{2}$ as a choice proposed by Chaudhary-Bathe [6], the energy change is

$$[^tE] = <^t \mathbf{R_c}>^T [^tU] - \frac{1}{4}\Delta t^2[\mathbf{T}(^t\ddot{U})] \tag{4.17}$$

$$\begin{aligned}
&= <^t \ddot{U}>^T \mathbf{M}[^tU] + <^t U> \mathbf{K}[^tU] \\
&\quad -\frac{1}{4}\Delta t^2(^{t+\Delta t}\ddot{U}^T\mathbf{M}^{t+\Delta t}\ddot{U} - ^t\ddot{U}^T\mathbf{M}^t\ddot{U})
\end{aligned} \tag{4.18}$$

In this case, the second term in equation (4.17) somehow compensates the energy change due to the average of the contact forces. Considering the relation (4.13), we can clearly see that the total energy of the system is conserved only for the case of a rigid body with no external force [6].

4.1.2 Bathe Method

For the Bathe method, we use a slightly different notation of the average and jump operators

$$< {}^{t}(X) >= 1/2({}^{t+\Delta t/2}(X) + {}^{t}(X)) \tag{4.19}$$

$$[{}^{t}(X)] = ({}^{t+\Delta t/2}(X) - {}^{t}(X)) \tag{4.20}$$

$$< {}^{t+\Delta t/2}(X) >= 1/2({}^{t+\Delta t}(X) + {}^{t+\Delta t/2}(X)) \tag{4.21}$$

$$[{}^{t+\Delta t/2}(X)] = ({}^{t+\Delta t}(X) - {}^{t+\Delta t/2}(X)) \tag{4.22}$$

As we studied in chapter 2, the Bathe method is a combination of the trapezoidal rule and the Euler 3-point backward method. One can calculate the total energy change in one time step by considering the energy change in each substep. For the first substep of the Bathe method, which is the trapezoidal rule, the equilibrium equation and the assumptions are

$$\mathbf{M}^{t+\Delta t/2}\ddot{U} + \mathbf{K}^{t+\Delta t/2}U = {}^{t+\Delta t/2}\mathbf{R_c} \tag{4.23}$$

$$\begin{aligned} {}^{t+\Delta t}\dot{U} &= {}^{t}\dot{U} + \frac{\Delta t}{2}({}^{t+\Delta t/2}\ddot{U} + {}^{t}\ddot{U}) && (4.24)\\ {}^{t+\Delta t}U &= {}^{t}U + \frac{\Delta t}{2}({}^{t+\Delta t/2}\dot{U} + {}^{t}\dot{U}) && (4.25) \end{aligned}$$

As in section 4.1.1, we can get the energy change as

$$[{}^{t}E] = <{}^{t}\mathbf{R_c}>^{T}[{}^{t}U] \tag{4.26}$$

For the second substep which is the Euler three point backward method, the equilibrium equation and the assumptions are

$$\mathbf{M}^{t+\Delta t}\ddot{U} + \mathbf{K}^{t+\Delta t}U = {}^{t+\Delta t}\mathbf{R_c} \tag{4.27}$$

$$\begin{aligned} {}^{t+\Delta t}\dot{U} &= \frac{3}{\Delta t}{}^{t+\Delta t}U - \frac{4}{\Delta t}{}^{t+\Delta t/2}U + \frac{1}{\Delta t}{}^{t}U \\ &= \frac{3}{\Delta t}[{}^{t+\Delta t/2}U] - \frac{1}{\Delta t}[{}^{t}U] && (4.28) \end{aligned}$$

$$
\begin{aligned}
{}^{t+\Delta t}\ddot{U} &= \frac{3}{\Delta t}\,{}^{t+\Delta t}\dot{U} - \frac{4}{\Delta t}\,{}^{t+\Delta t/2}\dot{U} + \frac{1}{\Delta t}\,{}^{t}\dot{U} \\
&= \frac{3}{\Delta t}[{}^{t+\Delta t/2}\dot{U}] - \frac{1}{\Delta t}[{}^{t}\dot{U}] \qquad (4.29)
\end{aligned}
$$

The total energy change of the system is obtained by calculating the change of the kinetic energy and the strain energy as before

$$
[\mathbf{T}({}^{t+\Delta t/2}\dot{U})] = [{}^{t+\Delta t/2}\dot{U}]^T\mathbf{M} <{}^{t+\Delta t/2}\,\dot{U}> \qquad (4.30)
$$

$$
[\mathbf{V}({}^{t+\Delta t/2}U)] = [{}^{t+\Delta t/2}U]^T\mathbf{K} <{}^{t+\Delta t/2}\,U> \qquad (4.31)
$$

We can simplify the sum of the equations (4.30) and (4.31) using following relations

$$
\begin{aligned}
[{}^{t+\Delta t/2}\dot{U}] &= \frac{\Delta t}{3}\,{}^{t+\Delta t}\ddot{U} + \frac{1}{3}[{}^{t}\dot{U}] \\
&= \frac{\Delta t}{3}(<{}^{t+\Delta t/2}\,\ddot{U}> + \frac{1}{2}[{}^{t+\Delta t/2}\ddot{U}] + \frac{1}{\Delta t}[{}^{t}\dot{U}]) \qquad (4.32) \\
<{}^{t+\Delta t/2}\,\dot{U}> &= {}^{t+\Delta t}\dot{U} - \frac{1}{2}[{}^{t+\Delta t/2}\dot{U}] \\
&= \frac{3}{\Delta t}([{}^{t+\Delta t/2}U] - \frac{1}{3}[{}^{t}U] - \frac{\Delta t}{6}[{}^{t+\Delta t/2}\dot{U}]) \qquad (4.33)
\end{aligned}
$$

$$
[{}^{t}U] = \frac{\Delta t}{2} <{}^{t}\,\dot{U}> \qquad (4.34)
$$

$$
[{}^{t}\dot{U}] = \frac{\Delta t}{2} <{}^{t}\,\ddot{U}> \qquad (4.35)
$$

$$
<{}^{t+\Delta t/2}\,\ddot{U}>^T \mathbf{M}[{}^{t+\Delta t/2}U] + <{}^{t+\Delta t/2}\,U>^T \mathbf{K}[{}^{t+\Delta t/2}U] = <{}^{t+\Delta t/2}\,\mathbf{R_c}>^T [{}^{t+\Delta t/2}U] \qquad (4.36)
$$

After some algebra, we obtain

$$
\begin{aligned}
[{}^{t+\Delta t/2}E] &= [\mathbf{T}({}^{t+\Delta t/2}\dot{U})] + [\mathbf{V}({}^{t+\Delta t/2}U)] \\
&= <{}^{t+\Delta t/2}\,\mathbf{R_c}>^T [{}^{t+\Delta t/2}U] \\
&\quad -\frac{1}{2}([{}^{t+\Delta t/2}\dot{U}]^T + <{}^{t}\,\dot{U}>^T)\mathbf{M}[{}^{t+\Delta t/2}\dot{U}] \\
&\quad +\frac{1}{2}([{}^{t+\Delta t/2}\ddot{U}]^T + <{}^{t}\,\ddot{U}>^T)\mathbf{M}[{}^{t+\Delta t/2}U] \qquad (4.37)
\end{aligned}
$$

We can also find that the difference between the second term and the third term is of order Δt^2. Therefore, the equation above can be expressed as

$$[^{t+\Delta t/2}E] = <^{t+\Delta t/2}\mathbf{R_c}>^T [^{t+\Delta t/2}U] - O(\Delta t^2) \tag{4.38}$$

Finally, the total energy change in one time step of the Bathe method is

$$[^tE] + [^{t+\Delta t/2}E] = <^t\mathbf{R_C}>^T [^tU] + <^{t+\Delta t/2}\mathbf{R_C}>^T [^{t+\Delta t/2}U] - O(\Delta t^2) \tag{4.39}$$

As we can see, the energy change in the solution of the Bathe method is similar to the energy change in the solution of the trapezoidal rule and the Bathe method introduces little numerical damping. From the investigations of the energy change of the total system in each time step, we can see that the average of the contact forces causes the energy change in implicit dynamic simulations. In the following subsection, we assess the effect of the contact force in detail.

4.1.3 Effect of the contact force on the total energy of the system

As we saw in the previous subsection, the contact force affects the total energy of the system in each time step as

$$[^tE]_c = <^t\mathbf{R_c}>^T [^tU] \tag{4.40}$$

For the simple case, using the notation in ref [4], the contact force $\mathbf{R_c}$ can be expressed as

$$\mathbf{R_c} = \mathbf{K}_\lambda \lambda \tag{4.41}$$

where the matrix $\mathbf{K}_\lambda$ is the contact matrix which includes the geometrical information to transform the scalar Lagrange multiplier vector, λ, to a physical force and the

appropriate connectivity information. Also, we can describe the gap function, g, as

$$g = \mathbf{K}_\lambda{}^T U + g_0 \tag{4.42}$$

where the admissible condition of contact is

$$g_i \geqq 0 \tag{4.43}$$

$$\lambda_i \geqq 0 \tag{4.44}$$

$$g_i \lambda_i = 0 \tag{4.45}$$

We refer to reference [1] for a detailed explanation of the above conditions. With the equations (4.41) and (4.42), we can express the energy change, $[{}^tE]_c$ as

$$[{}^tE]_c = <{}^t\mathbf{R_c}>^T [{}^tU] \tag{4.46}$$

$$= \frac{1}{2}({}^{t+\Delta t}\mathbf{K}_\lambda{}^{t+\Delta t}\lambda + {}^t\mathbf{K}_\lambda{}^t\lambda)^T({}^{t+\Delta t}U - {}^tU) \tag{4.47}$$

If we assume that the contact matrix $\mathbf{K}_\lambda$ is constant in one time step, the above equation is simplified to

$$[{}^tE]_c = \frac{1}{2}({}^{t+\Delta t}\lambda + {}^t\lambda)^T\mathbf{K}_\lambda^\mathbf{T}({}^{t+\Delta t}U - {}^tU) \tag{4.48}$$

$$= \frac{1}{2}({}^{t+\Delta t}\lambda + {}^t\lambda)({}^{t+\Delta t}g - {}^tg) \tag{4.49}$$

$$= \frac{1}{2}\sum_{i=1}^{n}({}^{t+\Delta t}\lambda_i + {}^t\lambda_i)({}^{t+\Delta t}g_i - {}^tg_i) \tag{4.50}$$

With equation (4.50), we can evaluate $[{}^tE]_c$ of three different states in the contact events : new contact step, continuous contact step and releasing step.

New contact step

When contact appears in the current time step, we have ${}^{t+\Delta t}\lambda > 0$ and ${}^t\lambda = 0$. Also, from the contact condition (4.43) and (4.45), we notice that ${}^{t+\Delta t}g = 0$ and ${}^tg > 0$. Therefore, in the this contact step, $[{}^tE]_c < 0$ (Energy decreasing)

Continuous contact step

During the step when the contact forces exist both in the previous time and the current time, then ${}^{t+\Delta t}\lambda > 0$ and ${}^{t}\lambda > 0$. Therefore, ${}^{t+\Delta t}g = 0$ and ${}^{t}g = 0$. Therefore, $[{}^{t}E]_c = 0$. (Energy is conserved)

Releasing step

In the step when contact disappears, ${}^{t+\Delta t}\lambda = 0$ and ${}^{t}\lambda > 0$. Also, from the contact conditions, we find that ${}^{t+\Delta t}g > 0$ and ${}^{t}g = 0$. Therefore, in the releasing step, $[{}^{t}E]_c > 0$. (Energy increasing)

One may notice that the amount of the decreased energy and the increased energy are different in general. Also, for stability, we want to avoid the energy increasing step. It should be noticed that the contact force in the previous time in the releasing step makes the energy increasing. In the next section, a simple implicit method is proposed which eliminates the increased energy by eliminating the contact force ${}^{t}\lambda$ in every contact step using the concept of the momentum exchange. Furthermore, we can compensate the decreased energy in the new contact time by consideration of work done by the internal force and contact force while applying the contact constraints.

4.2 A simple implicit contact algorithm for energy-momentum conservation

4.2.1 Contact problem solutions using impulses

There is another way to approach contact and impact problems other than enforcing contact constraints, which is expressed in terms of location and contact forces. In this category, the methods treat contact forces as if they occur instantaneously, namely, methods treat the contact forces as impulses [10]. In this way, the contact forces change momentum directly instead of treating the momentum change as a result of

changes in acceleration.

If two bodies, 1 and 2, approach along the direction $\hat{n}$, conservation of the momentum give us the relation between the post-collision velocities, v_{1f}, v_{2f}, and pre-collision velocities v_1, v_2 as following.

$$(v_{1f} - v_{2f}) \cdot \hat{n} = -e(v_1 - v_2) \cdot \hat{n} \tag{4.51}$$

where e is the coefficient of restitution of the collision. And the impulse in this collision can be expressed as

$$v_{1f} = v_1 - \frac{J}{m_1}\hat{n} \tag{4.52}$$

$$v_{2f} = v_2 + \frac{J}{m_2}\hat{n} \tag{4.53}$$

$$J = \frac{(1+e)(v_1 - v_2)\hat{n}}{\frac{1}{m_1} + \frac{1}{m_2}} \tag{4.54}$$

One may notice that this impulse acts only in the normal direction of the collision, $\hat{n}$. Therefore, it can be separated from the tangential sliding direction [7]. In the following sections, we revisit the concept of the decomposed impulse which is introduced in [7], and then we introduce an implicit method which basically combines the conventional Lagrange multiplier method with the approach, which deals with contact problems in impulsive nature. The method is quite stable and accurate by eliminating the computationally generated energy by contact forces while it still efficient for practical usage.

4.2.2 Decomposed impulse

The momentum vector of all nodes involved in the contact can be expressed as

$$P = \mathbf{M}v \tag{4.55}$$

If the contact event occurred at time t_c, then the relation between the momentum vector in the post-impact state and the pre-impact state is

$$[P]_{t_c^-}^{t_c^+} = \Lambda \nabla g \tag{4.56}$$

where Λ is a scalar parameter. The energy conservation during the impact is described as

$$[P^T \mathbf{M}^{-1} P]_{t_c^-}^{t_c^+} = 0 \tag{4.57}$$

where the $\mathbf{M}^{-1}$ is used to obtain the energy. If the momentum vector just prior to the impact, $P_{t_c^-}$, is known, then we can get the momentum vector after the impact, $P_{t_c^+}$ using the above two equations. It should be noticed that this momentum in the post-impact state meets energy conservation as well as the total linear and angular momentum conservation. The above two equations lead to the following quadratic equation

$$(\Lambda \nabla g + P_{t_c^-})^T \mathbf{M}^{-1} (\Lambda \nabla g + P_{t_c^-}) - P_{t_c^+}^T \mathbf{M}^{-1} P_{t_c^+} = 0 \tag{4.58}$$

This quadratic equation is solved using iterative methods in [18] and was solved in closed form in [7] using the decomposition of the momentum. The momentum vector can be decomposed into normal and tangential components

$$P = P_n + P_t \tag{4.59}$$

where the normal component of the momentum vector is defined as orthogonal projection of the momentum vector onto the span of the gradient of the constraint function

$$\nabla g^T \mathbf{M}^{-1} P_t = 0 \tag{4.60}$$

We also have

$$\nabla g^T \mathbf{M}^{-1} (P - P_n) = 0 \tag{4.61}$$

Using the above equation, after some algebra, we find the expression for the normal component of the momentum vector

$$\nabla g^T \mathbf{M}^{-1} P_n = \nabla g^T \mathbf{M}^{-1} P \tag{4.62}$$

$$(\nabla g^T \mathbf{M}^{-1} P_n)\nabla g = (\nabla g^T \mathbf{M}^{-1} P)\nabla g \tag{4.63}$$

$$(\nabla g^T \mathbf{M}^{-1} \nabla g) P_n = (\nabla g^T \mathbf{M}^{-1} P)\nabla g \tag{4.64}$$

$$\therefore P_n = (\frac{\nabla g^T \mathbf{M}^{-1} P}{\nabla g^T \mathbf{M}^{-1} \nabla g})\nabla g \tag{4.65}$$

The momentum vectors at the post-impact state and the pre-impact state can be decomposed using the above definition

$$P^+ = P_t^+ + P_n^+ \tag{4.66}$$

$$P^- = P_t^- + P_n^- \tag{4.67}$$

One may notice that a momentum jump occurred only in the direction of ∇g from equation (4.56). Therefore, only the normal components are changed during the impact

$$P_t^+ = P_t^- \tag{4.68}$$

Also, the normal component of the momentum vector after the impact should be in the form $P_n^+ = C * P_n^-$ where C is constant, and $C = 1$ and $C = -1$ are the only solutions. Since $C = 1$ indicates a contact free solution, $C = -1$ is the solution. Therefore, the normal component of the momentum vector after the impact is

$$P_n^+ = -P_n^- \tag{4.69}$$

Therefore, the momentum vector after the impact is

$$P^+ = P_t^- - P_n^- \tag{4.70}$$

One may check that these results meet energy conservation

$$\frac{1}{2}P^{+T}\mathbf{M}^{-1}P^{+} - \frac{1}{2}P^{-T}\mathbf{M}^{-1}P^{-} = \Delta E \tag{4.71}$$

$$\frac{1}{2}(P_t^{+} + P_n^{+})^T\mathbf{M}^{-1}(P_t^{+} + P_n^{+}) - \frac{1}{2}(P_t^{-} + P_n^{-})^T\mathbf{M}^{-1}P^{-} = 0 \tag{4.72}$$

where $P_n^{-T}\mathbf{M}^{-1}P_t^{-} = 0$, $P_n^{+}\mathbf{M}^{-1}P_t^{+} = 0$

4.2.3 Procedure

From the analysis in chapter 4.1, we notice that contact forces can result into spurious energy dissipation and generation. There can be many ways to improve the solutions by adjusting the relationships between displacement, velocity, and acceleration to meet energy conservation in iterative ways [18][11][13]. However, when the contact is treated by impulses, and the velocity and acceleration are updated appropriately, we can meet energy consistency without changing any relationships.

In this subsection, we introduce a simple velocity and acceleration update process. In this approach, the enforcement of the impenetrability constraint and the exchange of the momenta during the contact events are considered separately. The configurations of the deformed bodies that follow the no-penetration condition and equilibrium are calculated by using conventional Lagrangian multiplier methods. At the end of each time step while contact events occur, the velocity and acceleration are updated by considering the contact events in an "impulsive nature".

To illustrate this updating process, a simple problem is considered in Figure 4-1. In this schematic problem, contact happens between the times t and $t + \Delta t$. The configuration of the deformed bodies at $t + \Delta t$ are taken from the usual Lagrangian method. In the solution process, the equations of motion are initially advanced to time $t + \Delta t$ without considering contact constraints $(t + \Delta t(-))$. Subsequently, the velocities of nodes that participate in the contact are updated by considering the impact that happened at that time $t + \Delta t(+)$ by using the methods described in chapter 4.2.2. Afterwards, these post-impact velocities are adjusted to meet the

energy conservation by considering the work done by the internal forces during the moving process to the configuration of the deformed bodies ($t + \Delta t(*)$). Lastly, the accelerations are updated to meet the equilibrium equation.

The work done by the internal forces during the moving process ($(+) \rightarrow (*)$) change the kinetic energy of the nodes. It also can be understood as enforcing that the sum of the strain energy and the kinetic energy should be conserved during the process

$$\int_{+}^{*} d(\frac{1}{2}\dot{U}^T M\dot{U}) = -\int_{+}^{*} Rd(U)$$

When we use the linear approximation about the work done by internal forces, the above equation becomes

$$^{*}\dot{U}^T M^{*}\dot{U} -^{+} \dot{U}^T M^{+}\dot{U} \backsimeq (^{*}U -^{+} U)^T(-^{*}R -^{+} R)$$

or

$$\sum_{i=1}^{n}\sum_{j=1}^{n} m_{ij}(^{*}v_i^{*}v_j -^{+} v_i^{+}v_j) \backsimeq \sum_{i=1}^{n}(^{*}u_i -^{+} u_i)(-^{*}r_i -^{+} r_i)$$

And if we use a lumped mass matrix, M_L, just for the update process,

$$\sum_{i=1}^{n} mL_{ii}(^{*}v_i^2 -^{+} v_i^2) \backsimeq \sum_{i=1}^{n}(^{*}u_i -^{+} u_i)(-^{*}r_i -^{+} r_i)$$

Finally, the adjusted post-impact velocity at node i can be approximated as follows.

$$^{*}v_i^2 =^{+} v_i^2 + \frac{1}{mL_{ii}}(^{*}u_i -^{+} u_i)(-^{*}r_i -^{+} r_i)$$

$$^{*}v_i = \frac{^{+}v_i}{|^{+}v_i|}[^{+}v_i^2 + \frac{1}{mL_{ii}}(^{*}u_i -^{+} u_i)(-^{*}r_i -^{+} r_i)]^{1/2}$$

In case the work done by the internal forces is negative, the sign of what is in the squared bracket can be negative when the amount of the work done by internal forces is larger than the initial kinetic energy of the node. Since the negative work means that the kinetic energy is transferred to the strain energy, physically the absolute amount of the work cannot be larger than the initial kinetic energy. However, since

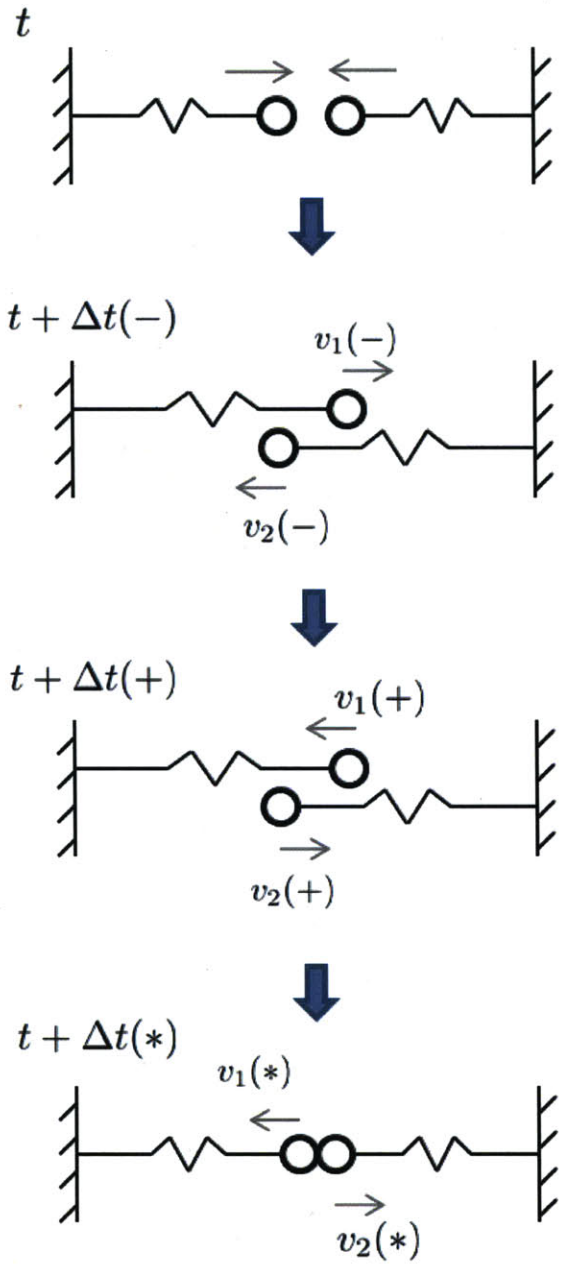

Figure 4-1: Process of the velocity and acceleration update

the deformed configurations are separately solved, this unwanted case rarely happens only when the time step size is too large. For simplicity of the simulation, the velocity of the node is set to zero when the sign of what is in the bracket is negative and when this situation happens, the energy of the system is increased by the absolute value of what is in the bracket.

4.2.4 Numerical examples

This subsection presents a few results obtained with two widely used implicit time integration methods, the trapezoidal rule and the Bathe method with the proposed update algorithm, giving comparisons also with results obtained using the trapezoidal rule, the Bathe method and Chaudhary-Bathe method without the update process.

1-D spring problem

First, the one dimensional impact of two point masses attached to the springs is considered, as depicted in Figure 4-2. In this problem, the two masses have the same equilibrium point at the origin. Initially, mass 1 is displaced to -5, moving at a velocity of -3 and mass 2 is displace to 2 and moving at a velocity of 1. The properties are: $m_1 = 2$, $m_2 = 1$, $k_1 = 3$ and $k_2 = 8$, all in appropriate units.

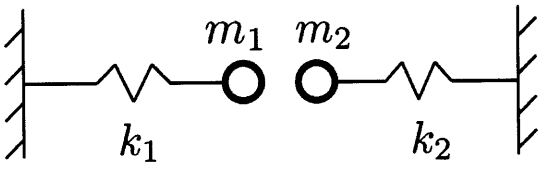

Figure 4-2: 1-D spring problem

Before doing the numerical simulations, we check the reliability of the code developed in this research by comparing the results with ADINA results. Figure 4-3 shows that the results match well. The numerical solutions are obtained with two time step sizes, $\Delta t = 0.01, 0.05$. We consider five methods for the temporal integrations: the trapezoidal rule with and without the update process, the Bathe method with and without update process and Chaudhary-Bathe method. Solutions for these cases are shown in Figure 4-4. The results show that the trapezoidal rule without

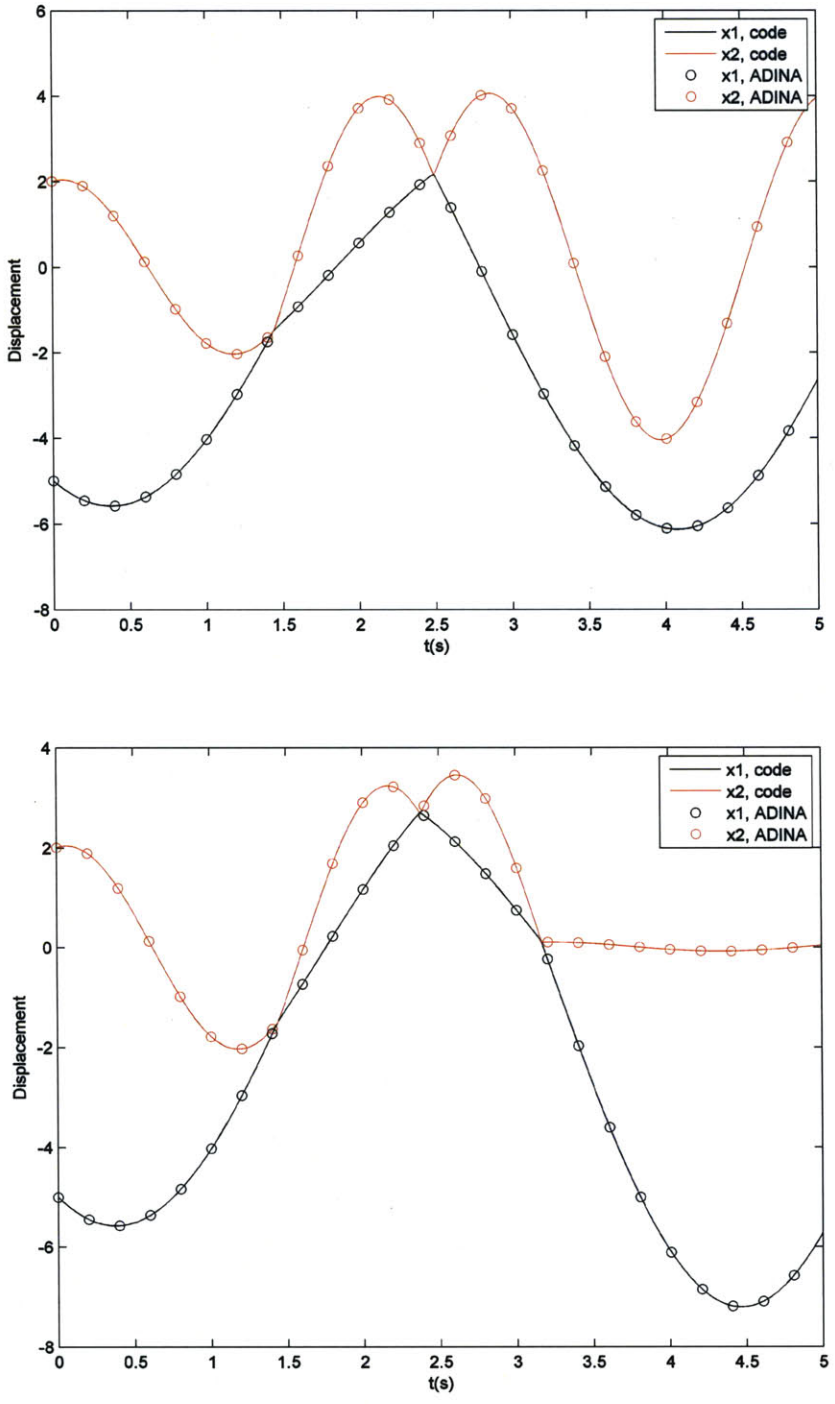

Figure 4-3: Displacement of the balls for the Newmark method (the trapezoidal rule) and the Bathe method

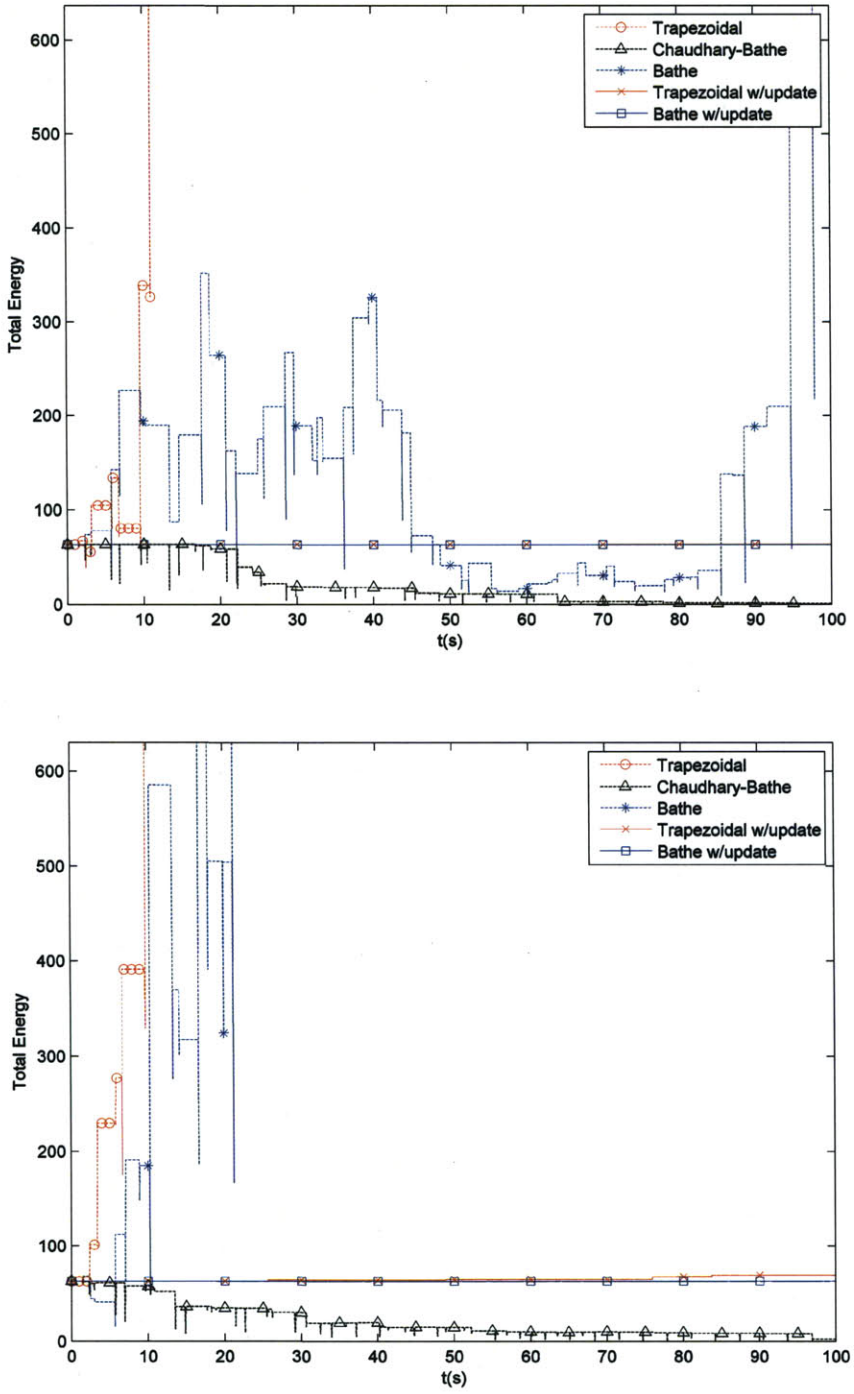

Figure 4-4: Total energy vs. time in the 1-D impact problem for $\Delta t = 0.01, 0.05$

update process and the Bathe method without update process produce spurious energy in contact events so that the results blow up after first few impacts. In contrast to the previous two methods, Chaudhary-Bathe method algorithmically compensates the spuriously dissipated and generated energy well in the first few contact events, so that a reasonable solution is produced. However, the solution starts to dissipate the system energy in the contact events and the response eventually damps out.

Notably, the simple update process significantly enhances the responses predicted by both time integration methods, the trapezoidal rule and the Bathe method. Both methods conserve the total energy when combined with the update process for a long time when the small time step size is used. However, when the time step size becomes bigger, the nonphysical situation, which is described in chapter 4.2 happens in the solution of the trapezoidal rule with the update, so the total energy is increased. It is worth to mention that the small numerical dissipation in the Bathe method prevents this nonphysical situation so it also conserves the total energy well for the $\Delta t = 0.05$ case.

The Carom problem

The two dimensional Carom problem, or billiard pool problem, involves perfectly elastic and frictionless impact. The problem consists of the analysis of a single ball trajectory and total energy in the ten-unit square rigid box. The ball is modeled by one nine-node element. An initial velocity $V_0 = (1, -1)$ unit and a position $(-2.25, -2.25)$ unit are prescribed. The material properties and the dimensions are as follows : Young's modulus $E = 10^3$ unit, Poisson's ratio $\nu = 0.0001$, density $\rho = 1$ unit and diameter $d = 1$ unit. The time step size $\Delta t = 0.01$ unit is utilized in each simulation, performed using the five methods as in the previous example. The initial condition causes the ball to hit the lower side at the middle and at an angle of 45 degree.

The results in Figure 4-5, show that in case of the trapezoidal rule without the update process, the first rebound is too sharp due to gain of energy. Although the trapezoidal rule is unconditionally stable for linear problems, it is unstable due to

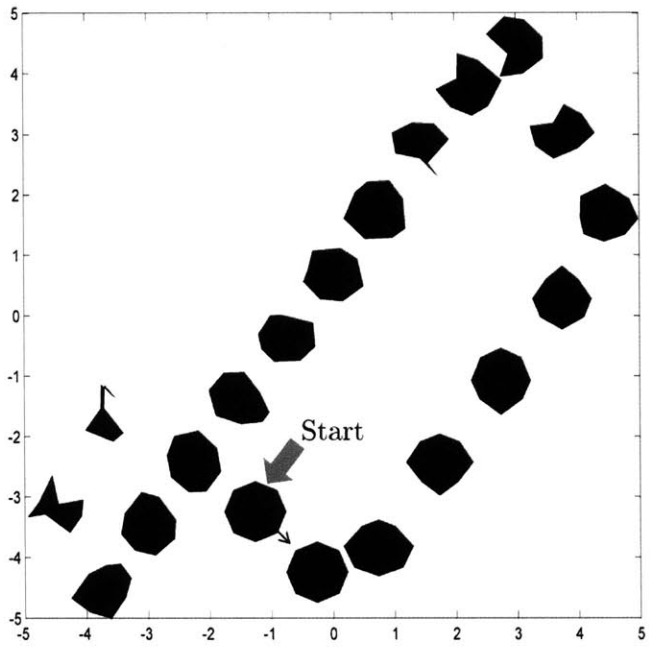

Figure 4-5: The 2-D Carom problem : ball position at every second for the trapezoidal rule without the update

the contact nonlinearities, which generate spurious energy at every contact and it eventually blows up. The results from the Bathe method also shows similar effect due to the spurious energy gain (Figure 4-6) but it gives a stable result. The Chaudhary-Bathe methods has the opposite effect, with the angle of rebound being flat and the system energy being reduced. However, since the method is designed to conserve total energy for the rigid body impact, the amount of the spuriously dissipated energy is not severe(Figure 4-7). Finally, the results from the methods with the update process (Figure 4-8, 4-9) show that both methods generate energy in every contact. This is mainly from the linear approximation of the work done by the internal forces, however, the amount of the generated energy is not severe. Notably, the Bathe method with the update process predicts all rebounds to be about 45 degree, giving the expected almost square-shaped trajectory of the ball within the carom board.

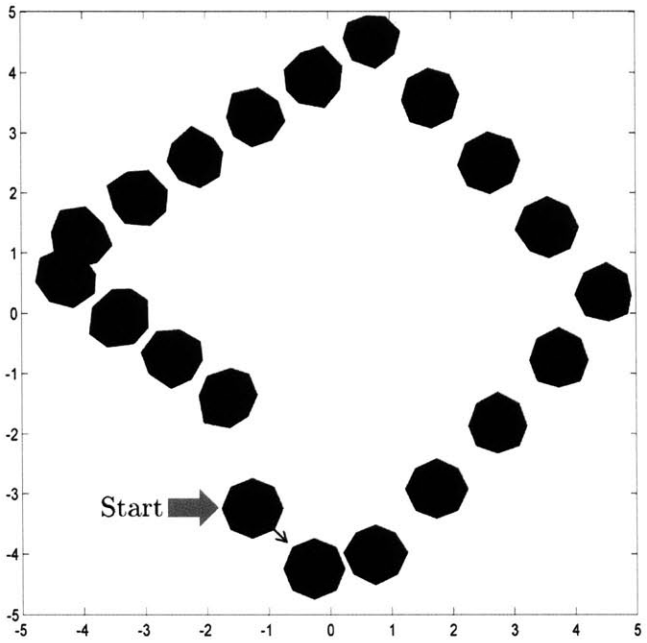

Figure 4-6: The 2-D Carom problem : ball position at every second for the Bathe method without the update

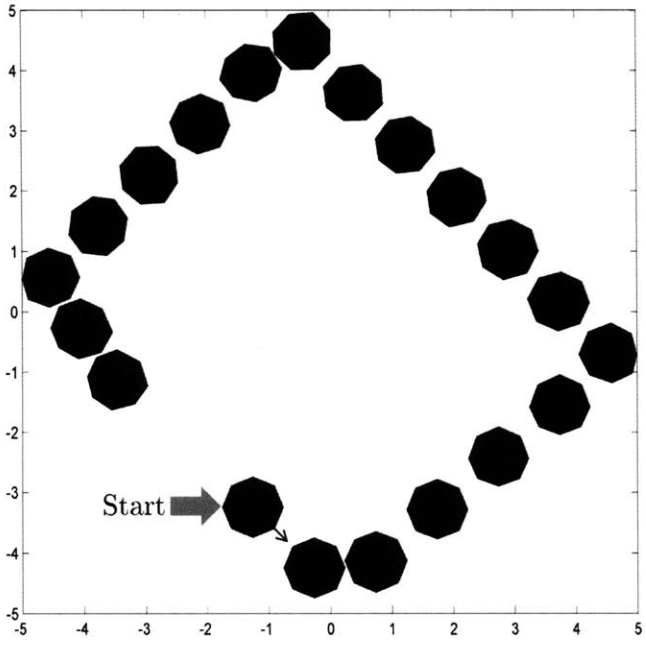

Figure 4-7: The 2-D Carom problem : ball position at every second for the Chaudhary-Bathe method without the update

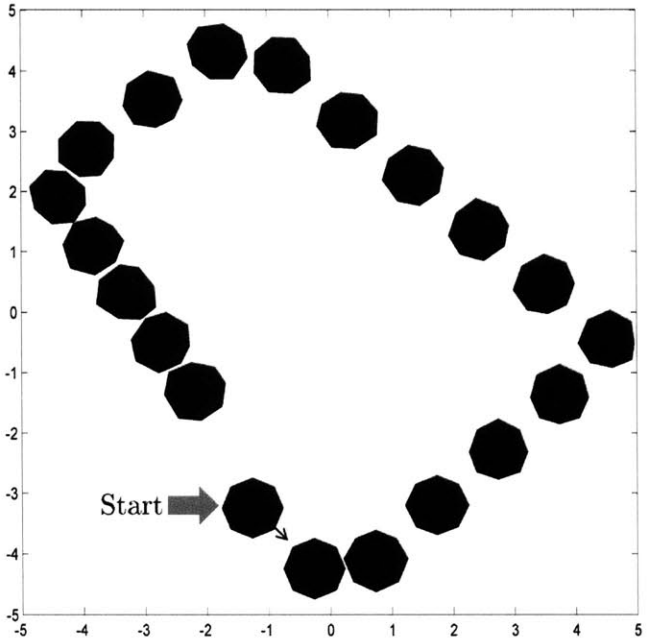

Figure 4-8: The 2-D Carom problem : ball position at every second for the trapezoidal rule with the update

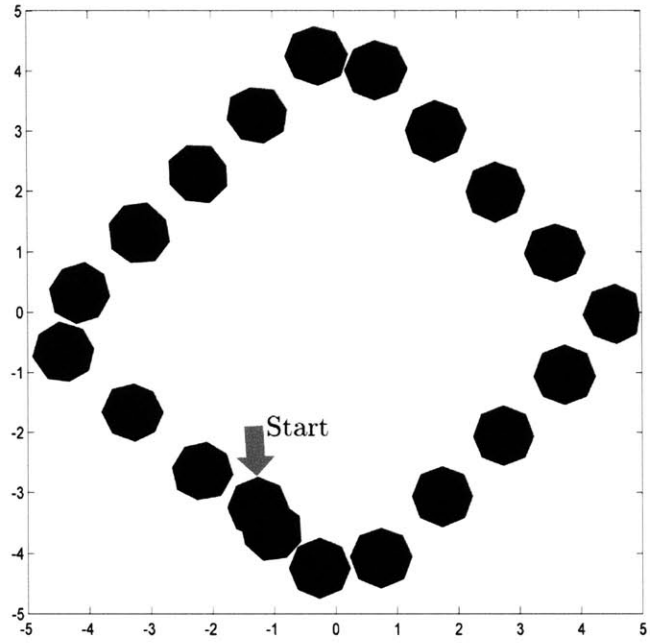

Figure 4-9: The 2-D Carom problem : ball position at every second for the Bathe method with the update

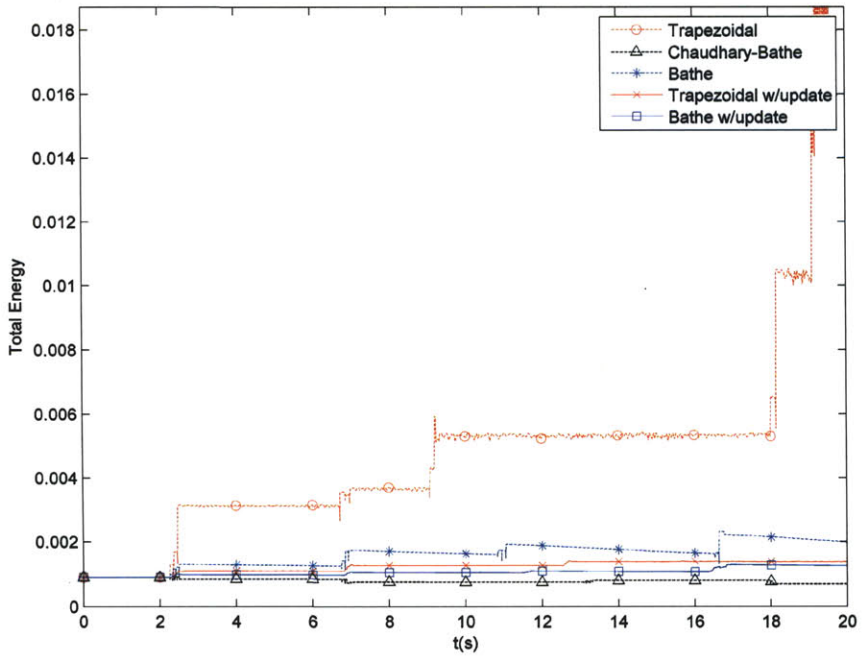

Figure 4-10: The 2-D Carom problem : total energy vs. time for the five methods

2-D Block impact problem

In this subsection, a soft block impact problem is solved to see how the stress field is affected by the update process. The problem consists of the analysis of the total energy of the block and the stress propagations. The block is modeled by a linear elastic material and the floor is a fixed rigid body. The block has a rectangular shape of (0.4, 0.6) units and is discretized by 96, four node, squared shaped elements. The simulation parameters are as follows: Young's modulus $E = 200$ unit, Poisson's ratio $\nu = 0.3$, density $\rho = 1$ unit and the initial velocity $V_0 = (3.5, -1.5)$ units is prescribed. The time step size $\Delta t = 0.01$ is used.

The results in Figure 4-11, show that every method provides satisfactory results in terms of the total energy. However, although the system energy is equivalent in the results, it is not trivial that solutions have similar stress wave propagations. Since the update process is applied to the nodes participating contact events, it might cause stress concentration around the surface during the contact events. Figures 4-12, 4-13

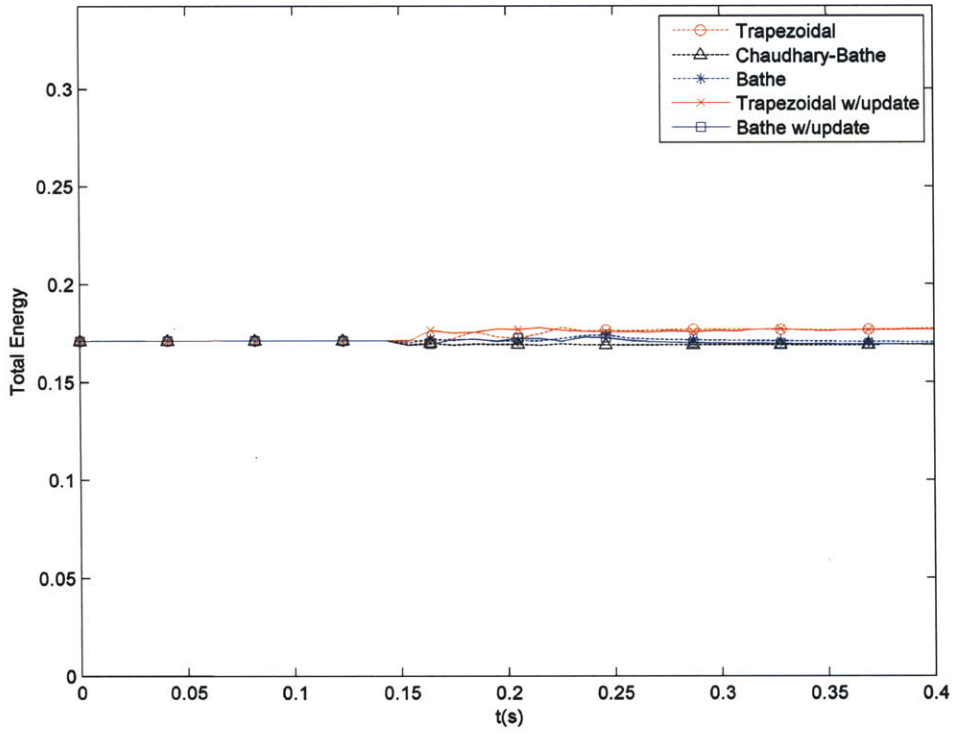

Figure 4-11: The 2-D block impact problem : total energy vs. time for the five methods

present the history of the von Mises stress in the blocks every 0.02 time unit of the Bathe method with the update process and without the update process and it is seen that the stress fields are almost the same.

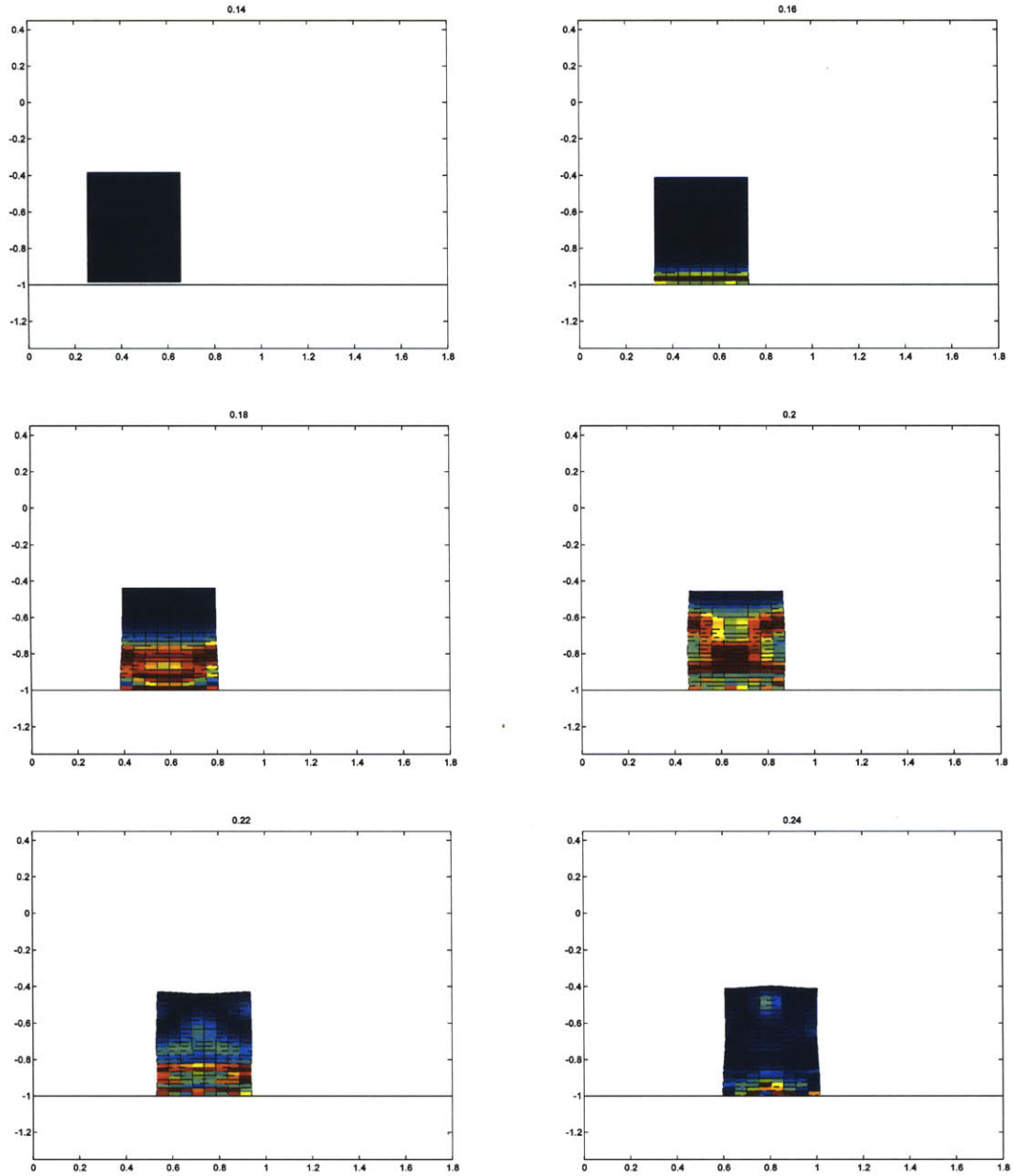

Figure 4-12: History of the von Mises stress for the Bathe method without update process in every 0.02 time units (t = from 0.14 to 0.24)

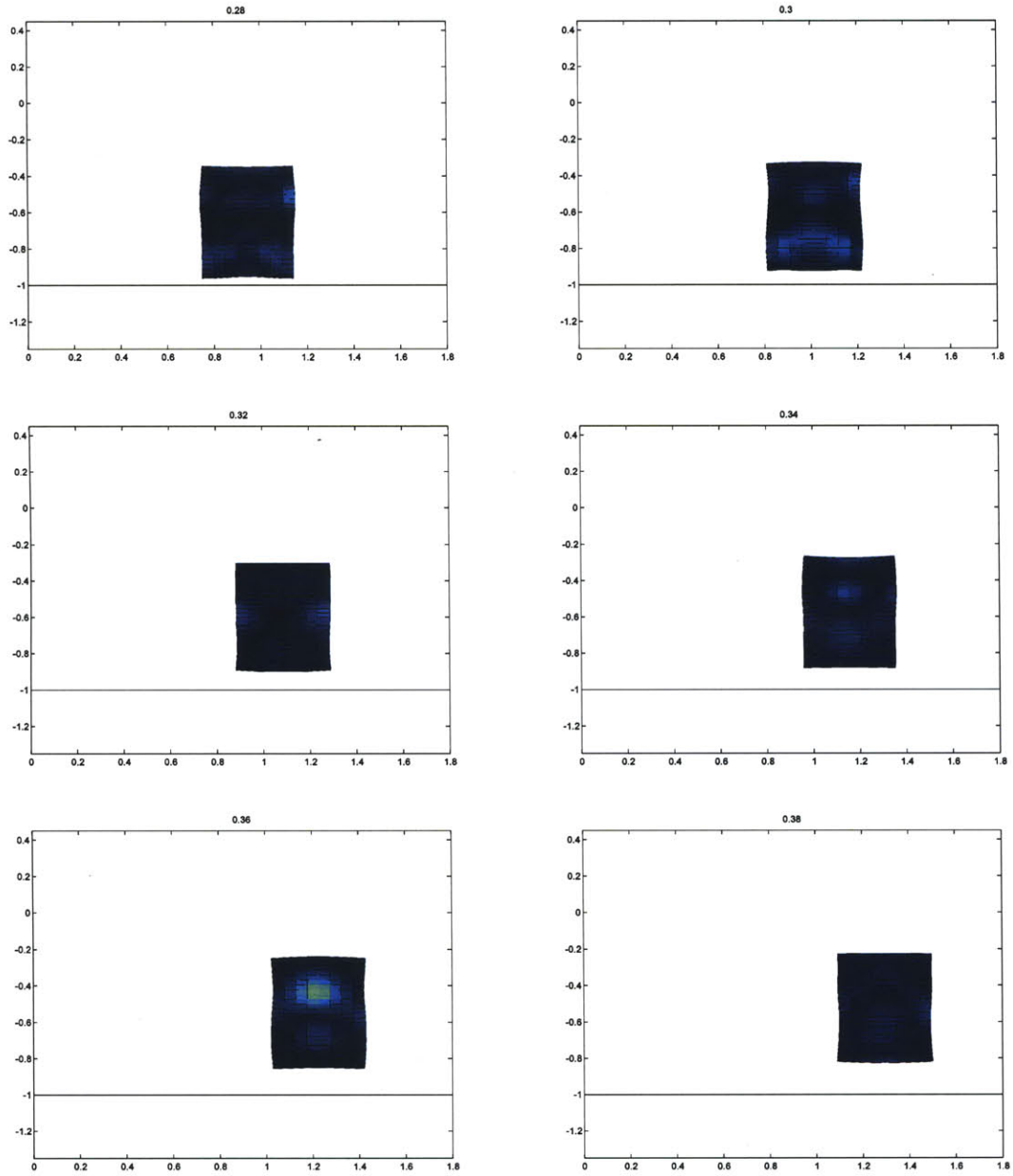

Figure 4-13: History of the von Mises stress for the Bathe method without update process in every 0.02 time units (t = from 0.28 to 0.38)

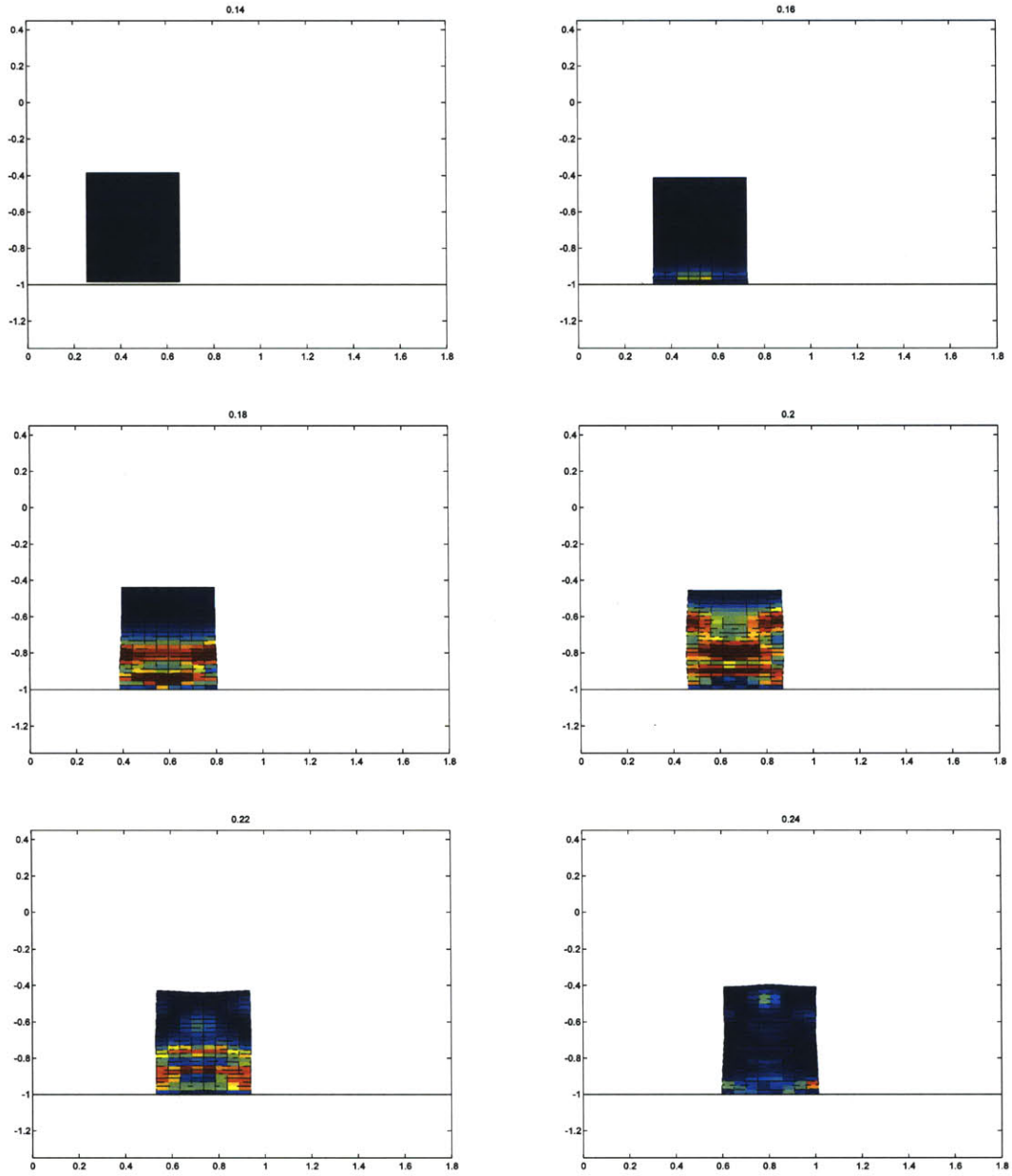

Figure 4-14: History of the von Mises stress for the Bathe method with update process in every 0.02 time units (t = from 0.14 to 0.24)

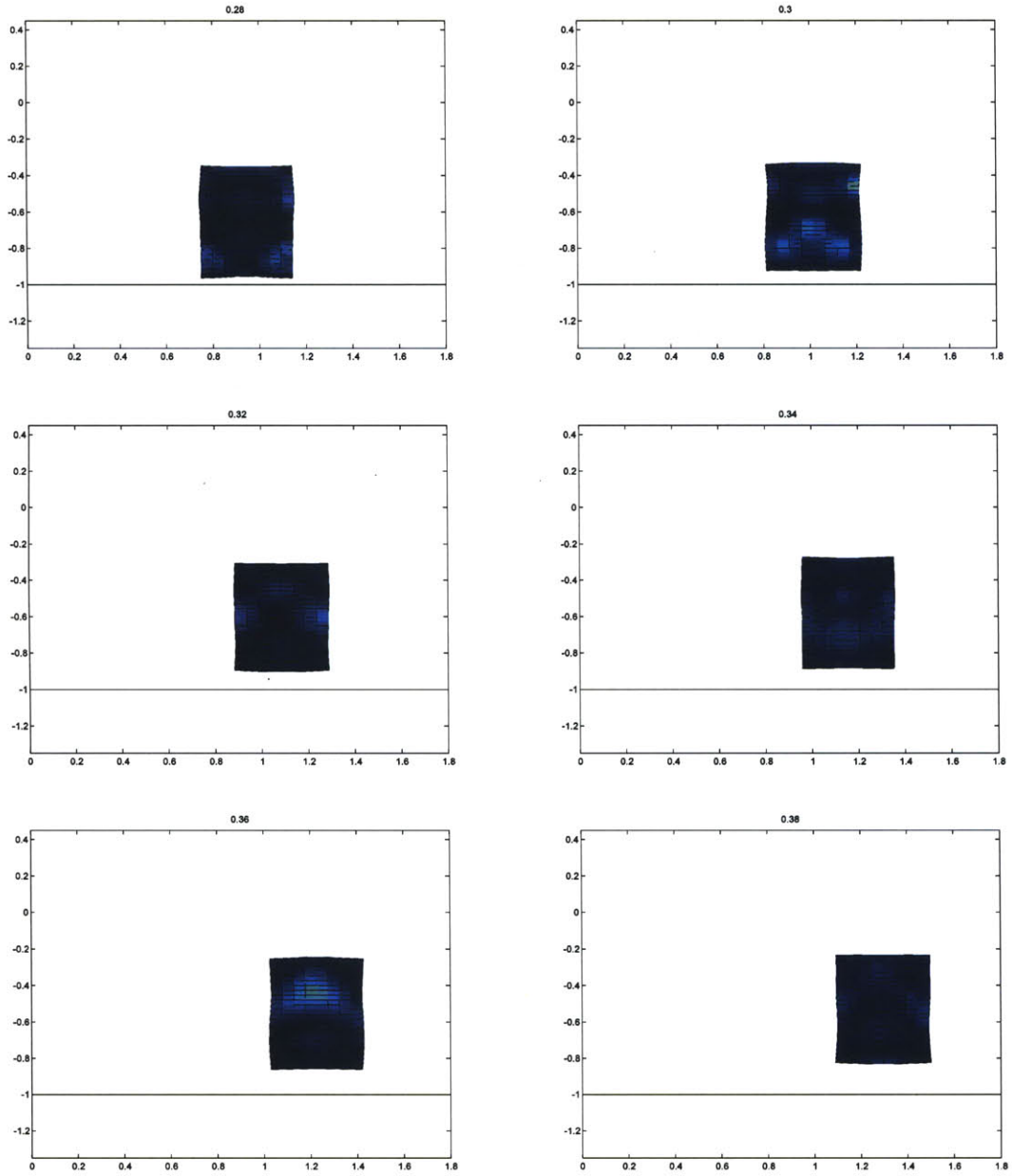

Figure 4-15: History of the von Mises stress for the Bathe method with update process in every 0.02 time units (t = from 0.28 to 0.38)

Chapter 5

Summary

We evaluated accuracy and stability characteristics of time integration schemes for contact problems. The presentation can be summarized as follows:

- An analytical form of the time integration schemes' responses, in terms of amplitude decay and period elongation, is introduced. This analytical form can help to understand the characteristics of a method for contact problems. In this presentation, the contribution of the amplitude decay and period elongation on the error of the initial condition of the contact events is investigated.

- Using implicit time integration methods, which solve the equilibrium equations at discrete time points of interest, the contact force spuriously generates or dissipates energy. These variations of total energy are not compensated algorithmically without a general iteration process. The time integration schemes, which are unconditionally stable for linear problems, such as the trapezoidal rule, can be unstable due to this spuriously generated energy.

- The proposed update process, which makes a contact-free state by treating the contact events in an "impulsive nature", improves the response predicted by the implicit time integration methods. However, since it uses a linear approximation for the work done by internal forces and a lumped mass matrix, the response still has same small energy variation. Also, deformed configurations and post-impact velocities are separately obtained. Therefore, there can be a non-physical

situation that increases the system's energy when the time step size is too large.

- Results from the numerical examples show that when the update process is combined with the Bathe method, the small energy variations in the contact situations and the number of non-physical situations are minimized.

Bibliography

[1] K. J. Bathe. *Finite element procedures.* Prentice Hall, New York, 1996.

[2] K. J. Bathe. Conserving energy and momentum in nonlinear dynamics: A simple implicit time integration scheme. *Computers & Structures*, 85:437–445, 2007.

[3] K. J. Bathe and M. M. I. Baig. On a composite implicit time integration procedure for nonlinear dynamics. *Computers & Structures*, 83:2513–2524, 2005.

[4] K. J. Bathe and P. A. Bouzinov. On the constraint function method for contact problems. *Computers & Structures*, 64:1069–1085, 1997.

[5] K. J. Bathe and E. L. Wilson. Stability and accuracy analysis of direct integration methods. *Earthquake Engineering and Structural Dynamics*, 1:283–291, 1973.

[6] A. B. Chaudhary and K. J. Bathe. A solution method for static and dynamic analysis of three-dimensional contact problems with friction. *Computers & Structures*, 24:855–873, 1986.

[7] F. Cirak and M. West. Decomposition contact response for explicit finite element dynamics. *Int. J. for Num. Met. in Engng.*, 64:1078–1110, 2005.

[8] L. Collatz. *The numerical treatment of differential equations. 3rd ed.* Springer-Verlag, 1966.

[9] R. E. Bank W. M. Coughran R. K. Smith E. H. Grosse D. J. Rose, W. Fichter. Transient simulations of silicon devices and circuits. *IEEE Trans CAD*, 4:436–51, 1985.

[10] G. R. Fowles and G. L. Cassiday. *Analytical mechanics.* Thomson Brooks, 1962.

[11] C. Hesch and P. Betsch. A mortar method for energy-momentum conserving schemes in frictionless dynamic contact problems. *Int. J. for Num. Meth. in Engng.*, 77:1468–1500, 2009.

[12] T. J. R. Hughes. *The Finite Element Method: Linear Static and Dynamic Finite Element Analysis.* Prentice Hall, Englewood Cliffs, 1987.

[13] R. C. Getecau J. E. Marsden, M. Ortiz and M. West. Nonsmooth lagrangian mechanics and variational collision integrators. *SIAM J. Applied Dynamical Systems*, 2:381–416, 2003.

[14] M. Becker J. Spillmann and M. Teschner. Non-iterative computation of contact forces for deformable objects. *J. of WSCG*, 2007.

[15] D. Kuhl and M. A. Crisfield. Energy-conserving and decaying algorithms in non-linear structural dynamics. *Int. J. Numer. Meth. Engng.*, 45:569–599, 1999.

[16] S. Erlicher L. Bonaventura, O. S. Bursi. The analysis of the generalized alpha method for non-linear dynamic problems. *Computational Mechanics*, 28:83–104, 2002.

[17] F. J. Wang L. P. Wang, J. G. Cheng and Z. H. Yao. Contact force algorithm in explicit transient analysis using finite-element method. *Finite Elements in Analysis and Design*, 43:580–587, 2007.

[18] G. R. Love and T. A. Laursen. Improved implicit integrators for transient impact problems-dynamic frictional dissipation within an admissible conserving framework. *Computer Methods in Applied Mechanics and Engng.*, 192:2223–2248, 2003.

[19] J. C. Simo N. Tarnow, K. K. Wong. Exact energy-momentum conserving algorithms and symplectic schemes for nonlinear dynamics. *Comp. Meth. in App. Mechanics and Engng.*, 100:63–116, 1992.

[20] H. B. Khenous P. Laborde, Y. Renard. Comparison of two approaches for the discretization of elastodynamic contact problems. *Mathematical Problems in Mechanics*, pages 791–796, 2006.

[21] H. B. Khenous P. Laborde, Y. Renard. Mass redistribution method for finite element contact problems in elastodynamics. *European Journal of Mechanics A/Solids*, 27:918–932, 2008.

[22] M.A. Puso and E. Zywicz. Energy and momentum conserving algorithms for rigid body contact. *Int. Conference on Computational Engng. Sci.*, 1998.

[23] W. T. M. Silva and L. M. Bezerra. Performance of composite implicit time integration scheme for nonlinear dynamic analysis. *Mathematical Problems in Engng.*, 2008.

[24] S. Dharmaraja Y.Wang, G. Strang. Optimal stability for trapezoidal-backward difference split-steps. *IMA J. of Numerical Analysis Advance Access*, pages 1–8, 2009.

[25] O. C. Zienkiewicz and J. Z. Zhu. A simple error estimator and adaptive procedure for practical engineering analysis. *Int. J. for Numer, Met. in Engng.*, 24:337–357, 1987.